Experimental Investigations on pressure pulses through different porous media

by

Gianlucca Nicolaico

A thesis submitted to the Graduate Faculty of
Auburn University
in partial fulfillment of the
requirements for the Degree of
Master of Science

Auburn, Alabama
December 9, 2023

Keywords: Transient flows, Porous Media, Hyperbolic PDE, Parabolic PDE, Solenoid Valve.

Approved by
Jose G. Vasconcelos, Chair, Associate Professor of Civil Engineering
Xing Fang, Professor of Civil Engineering
Frances O'Donnell, Assistant Professor of Civil Engineering

Abstract

Fluid mechanics traditionally and significantly investigate transient flows, which find applications ranging from flows in pipelines to porous media flows linked to water extraction and hydrocarbons. However, the nature of transient flows in closed pipes and porous media differs significantly due to the magnitude of energy losses in these two flows. Pipe systems experience relatively low energy dissipation rates, and one can describe them using partial differential equations (PDEs), such as the classic wave equation, which exhibit a hyperbolic nature. On the other hand, porous media flows are dominated by energy losses, and sudden changes associated with transient flows propagate gradually, exhibiting behavior similar to diffusion, characterized by parabolic-type PDEs. Although experiments have extensively investigated each of these flow conditions, they have yet to consider the transition between these two conditions, and there is a scarcity of transient flow datasets for highly conductive porous media.

The Water Resources Laboratory at Auburn University constructed an experimental apparatus to evaluate transient flow characteristics for six distinct porous media, each having unique diameters and materials. Each porous medium underwent evaluation for three different types of unsteady flows created by varying boundary conditions. The experimental findings revealed that transient signals gradually exhibited parabolic-type behavior as hydraulic conductivity decreased. In contrast, large porous media exhibited behavior consistent with closed pipe flows. The results indicate that the transition between these two regimes should be observed for porous media near or under a characteristic dimension of 2 mm.

Acknowledgments

Firstly, I would like to express my appreciation to the National Science Foundation for its sponsorship of this research. The support provided by the foundation has played a pivotal role in the successful completion of the present study.

I am sincerely grateful for the guidance and support provided by Doctor Vasconcelos as my esteemed advisor. I wish to particularly emphasize his exceptional intelligence, profound creativity, and unwavering patience in imparting knowledge. His mentorship has been instrumental in shaping the course of this endeavor.

I am grateful for the contributions of the members of my committee, Doctor Fang and Doctor O'Donnell. Their expertise and guidance played an important role in shaping my understanding of hydraulics and hydrology. Also, their constant solicitude and assistance have been invaluable throughout this academic journey.

My special thoughts go to my family, with special recognition to my grandmother Lizete whose kindness and resolute determination have consistently served as an inspirational force. Notably, her pursuit of undergraduate studies at the age of 50 stands as a testament to her remarkable spirit and fortitude.

Finally, and of equal significance, I express my profound gratitude to my friends, whom I regard as my second family, making my time in a foreign country feel just like home with all the emotional support they have shown me. During my stay in Auburn, I have been lucky to meet so many awesome people. It is hard to name everyone, so I will skip the specific names and give a shoutout to all of them for making a big impact on my life.

Table of Contents

List of Figures

List of Tables

1. Introduction

The relationship between human civilization and the utilization of porous media has endured for millennia, with evidence of its practical applications dating back to ancient times, even as far back as centuries B.C. (Angelakis et al. 2016). Porous media has applications in diverse fields, including agriculture, groundwater extraction, and the fuel cell industry (Brandon & Brett, 2006). However, the transition of porous media from an empirical knowledge base to a formal scientific discipline transpired primarily during the 19th Century, when the engineer Henry Darcy developed the first theories about the flow of fluids through porous materials (Baker et al.).

Since then, numerous studies have been developed to improve the knowledge around porous media encompassing diverse topics such as porosity characterization, multiphase flow phenomena, numerical simulations about porous media, and the investigation of transient flows within these intricate porous structures. This study emphasizes the characterization and examination of transient flows in porous media.

The description of transient flows in closed pipe systems, where porous media is absent, can be achieved by a system of mass and momentum conservation laws in the form of hyperbolic PDEs (Wylie et al. 1993). However, in the context of hydraulic transient flows within porous media, the nature of the flow variation is gradual, diffusive-like, and the mathematical description is performed through parabolic PDEs (Bear 1972). This difference comes from the dissimilarities created by energy losses between these two types of flows. Hyperbolic PDEs are appropriate for describing flows with a characteristic propagation speed (i.e., flow celerity) of pressure changes in the solution domain. Thus, closed pipe transients can present peak pressures in one location that can be detected in a location downstream after a short interval (e.g., milliseconds). By contrast, parabolic equations characterize gradual changes in flow conditions

similar to diffusive processes. Even when subjected to rapid changes in pressure conditions, the classical porous media flows will show gradual changes in pressure downstream from where transient flows started.

While each of these transient flows has been investigated numerically (Li et al. 2000; Tang et al. 2016; Pachaly et al. 2022) and experimentally (Soares et al. 2013, Urbanowicz et al. 2021, Zhou et al. 2021), there was no systematic study to evaluate conditions at the transition between these flows. The research questions that this work aims to address are two:

1) Would pressure changes during transient flows in porous media of large size behave like transient flows in closed pipes?
2) At what size would pressures in unsteady porous media flows begin to show the diffusive-like behavior that prevents observable transmission of pressure pulses?

1.1. Objectives

This research aims to study various rapidly-initiated unsteady flows in porous media to address the proposed research questions. Specifically, this study suggests:

- To create an experimental apparatus capable of generating hydraulic transient phenomena in closed pipes and porous media, with fast transient flow initiation via a solenoid valve.
- To conduct simulations of transient flows across various porous materials while characterizing these flows by acquiring high-frequency pressure data in the apparatus.
- To explore different transient flows by changing boundary conditions in the apparatus and compare as appropriate these results with available numerical modeling results.

2. Literature Review

The literature review includes two distinct categories of flow, specifically steady and transient flow in various media. In the case of transient flows, research has been conducted in porous media and in closed pipe applications. While this study primarily emphasizes transient flow in porous media, comprehending the fundamental concepts of transient pipe flows is essential. The investigation of steady flow phenomena in fluid systems relies on the widely accepted governing equation known as Darcy's Law, which has been extensively studied since the 19th Century. The comprehensive development of advanced theories related to transient flows emerged predominantly in the 20th Century. This advancement involved the solution of a system of partial differential equations to determine critical parameters, such as flow rate and piezometric head, at any point of a system at any given time.

2.1. Steady Flow in Porous Media

2.1.1. Porous Media Definition

In a rudimentary sense, porous media can be delineated as a collective assembly of solid particles and void spaces within a specified volumetric domain (Greenkorn 1983). However, the comprehension of this concept can be expanded and refined based on the specific level of analysis being pursued. At the microscopic scale, the concept of porous media is intimately associated with the characterization of pore structures and distribution sizes, while a macroscopic description centers on the bulk properties encompassing the entirety of the material, including permeability, dispersion, connectivity, and adsorption (Greenkorn 1983).

An accurate representation of the porous media is essential for computational modeling, enabling the simulation of real-life scenarios encompassing reactive transport (Hun et al., 2009),

geotechnical engineering (Grimstad et al., 2019), and petroleum engineering (Mehmani et al., 2014). Among different modeling approaches, it is included conceptual models for fractured media (Berre et al., 2019), finite difference models for groundwater equations such as MODFLOW (USGS, 2023), pore network models (Xiong et al. 2016), and others. Due to the relative similarity between pore network models and closed pipe flow models, some additional details are presented here on these models.

A pore structure model, or pore network model, is a tridimensional representation of the porous media that aims to accurately represent relevant properties of the domain, such as mechanical, thermal, and hydraulic (Song et al., 2023). Xiong et al. (2016) state that three distinct methodologies are conventionally employed to construct a pore network model: the first entails generating a statistically equivalent network by utilizing distributions associated with fundamental morphological and geometric parameters. The second method maps a network structure onto a designated void space within a porous medium. Lastly, the third approach is based on the diagenesis of porous media.

Haring and Greenkorn (1970) proposed a theoretical model to characterize the elemental pore space employing the statistical method cited by Xiong et al. (2016). Their representation considers each pore space as a collection of numerous randomly oriented straight cylindrical pores, assuming equal probability for all possible directions of a given pore (Figure 2.1). The parameters that describe each pore are radius (r), length (l), and spatial orientation angles (α_1, α_2). The domain of the model is $0 \leq r \leq R$, $0 \leq l \leq L$, $0 \leq \alpha_1 \leq \pi/2$, $0 \leq \alpha_2 \leq 2\pi$. Where R and L are respectively the largest pore and the longest pore in the control volume, respectively.

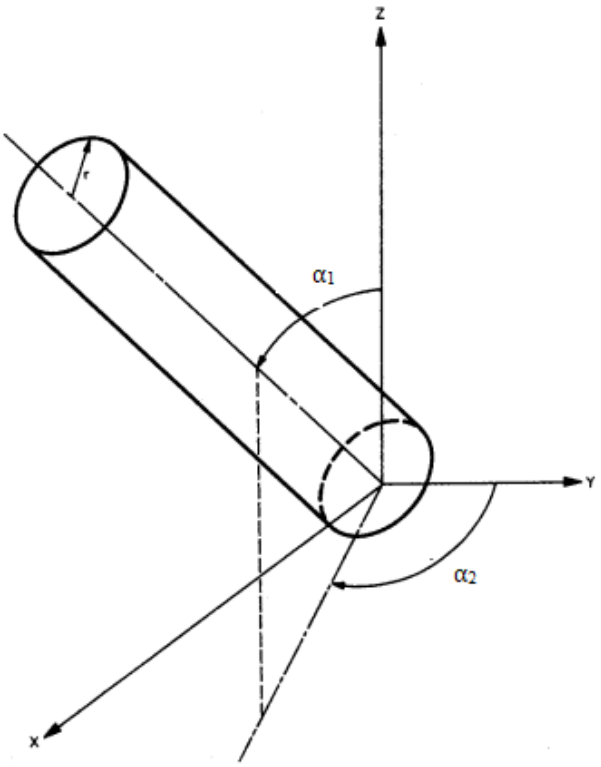

Figure 2.1: Description of elemental pore space (Guin et al. 1971)

The values of *r* and *l* are determined by using the following equations:

$$l = l^* * L \quad (2.1)$$

$$r = r^* * R \quad (2.2)$$

Where l^* and r^* are dimensionless parameters that vary from 0 to 1, according to the beta function distribution. Two parameters determine this function, and its shape depends on the uniformity of the porous medium. Figure 2.2 shows two possible beta functions: a uniform and a wide pore distribution.

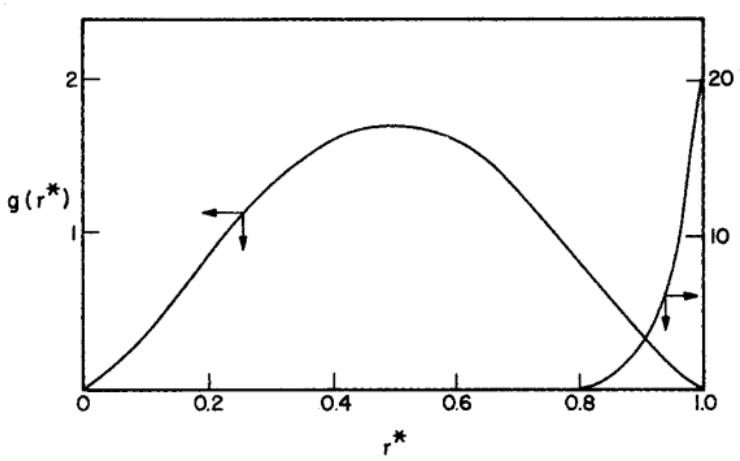

Figure 2.2: radius size distribution (Greenkorn 1983).

2.1.2. Darcy's Law

Porous media flow is a common and well-known phenomenon studied in many engineering and scientific applications. It is the flow of fluids through a porous media, such as soil, rocks, or aquifers. The study of porous media flow has been the subject of extensive research over the years, with most contributions focusing on the steady-state flow of fluids through porous media. Darcy investigated the flow of vertical sand filters connected to Dijon water fountains. His findings showed that the flow rate is directly proportional to the hydraulic gradient and the cross-sectional area, governed by the hydraulic conductivity or permeability of the porous medium, an intrinsic property of the ease with which fluids can flow through the medium (Bear 1979).

Despite the wide application of Darcy's Law, it has several assumptions and simplifications, including (Bear 1979):

- One-dimensional flow: The simplified version of Darcy's Law assumes that the fluid flows only in one direction. That type of representation is especially precise in systems like pipelines and water distribution networks.

- Incompressible Fluid: Darcy's Law assumes that the fluid flowing through the porous medium is incompressible, meaning its density remains constant during the flow. This assumption is appropriate for practical applications for most liquids, such as water.
- Homogeneous and Isotropic Media: Porous media properties (such as porosity and permeability) are assumed to be uniform throughout the media. Additionally, the medium is considered isotropic, meaning its properties are the same in all directions.
- Laminar Flow: fluid flow through the porous medium occurs in a laminar flow regime, where liquid particles move along well-defined flow paths without significant mixing or turbulence. This assumption is valid when the Reynolds number (a dimensionless parameter related to the flow regime) is sufficiently low.
- Single-Phase Flow: the presence of multiple phases, such as gas-liquid or immiscible fluids, is not considered in Darcy's Law.

Considering the assumptions above, Darcy's Law for a one-dimensional flow can be mathematically represented by the following formula:

$$Q = -KA\frac{dH}{dL} \tag{2.3}$$

Q is the fluid's volumetric flow rate through the porous media. K is the hydraulic conductivity of the porous media. A is the cross-sectional area perpendicular to the flow direction, and dh/dL is the hydraulic gradient, which is the change in hydraulic head per unit length along the flow direction.

2.1.3. Hydraulic Conductivity

Hydraulic Conductivity (*K*) is related to the capacity of a porous material to transmit fluids, such as water and oil. It depends on several factors, including porosity, particle size distribution, and fluid viscosity. Its dimension is (L/T); the most used units are m/s, cm/day, and in/min. There are several ways to estimate the hydraulic conductivity of a porous media. Some indirect methods include empirical formulas and mathematical models that predict hydraulic conductivity based on the physical properties of the soil.

Říha et al. (2018) conducted a comprehensive investigation encompassing a multitude of empirical formulas derived from experimental measurements and dimensional analysis to estimate the hydraulic conductivity of porous media comprising glass beads. After running 177 experimental tests, a statistical analysis was conducted to ascertain the validity and efficacy of each formula following the observed outcomes. The research findings concluded that the Terzaghi, Kozeny, and Zunker formulas emerge as the most accurate estimators for determining the hydraulic conductivity of glass beads. The respective formulations are presented below:

$$K = \frac{g}{\upsilon}\, C_r \left(\frac{n - 0.13}{\sqrt[3]{1-n}}\right)^2 {d_{10}}^2 \qquad 2.4$$

$$K = \frac{g}{\upsilon}\, C_{KO} \frac{n^3}{(1-n)^2}\, {d_e}^2 \qquad 2.5$$

$$K = \frac{g}{\upsilon}\, C_{ZU} \left(\frac{n}{1-n}\right)^2 {d_e}^2 \qquad 2.6$$

Where *K* is the porous media hydraulic conductivity, n is the porosity, g is gravitational acceleration, υ is the fluid viscosity, C_r is a constant that depends on the material shape, d_{10} is the grain diameter for 10% finer by weight, d_e is the effective grain size, C_{ZU} is an empirical coefficient that depends on the characteristics of the porous medium, and $C_{KO} = 8.3*10^{-3}$.

Direct methodologies also exist for measuring soil hydraulic conductivity within laboratory settings through permeameter tests (ASTM 2010). Such tests commonly involve the controlled application of pressure on a soil specimen, enabling the fluid flow rate measurement. The constant head and falling head tests are the most common permeability tests. In a constant head permeameter test, water is supplied at a constant pressure, and the flow rate is measured over time, whereas falling head tests run with an initial hydraulic head that drops as the water flows into the soil. In general, falling head tests are better suitable for low-permeability soils, while constant head tests apply to high-permeability soils due to the high flow rate commonly observed in those soils. The standardized procedure for conducting constant head and falling head permeameter tests can be referenced from the ASTM D5084 (2010) method.

Bear (1979) presented typical hydraulic conductivity values for porous media of different materials and particle sizes, shown in Figure 2.3.

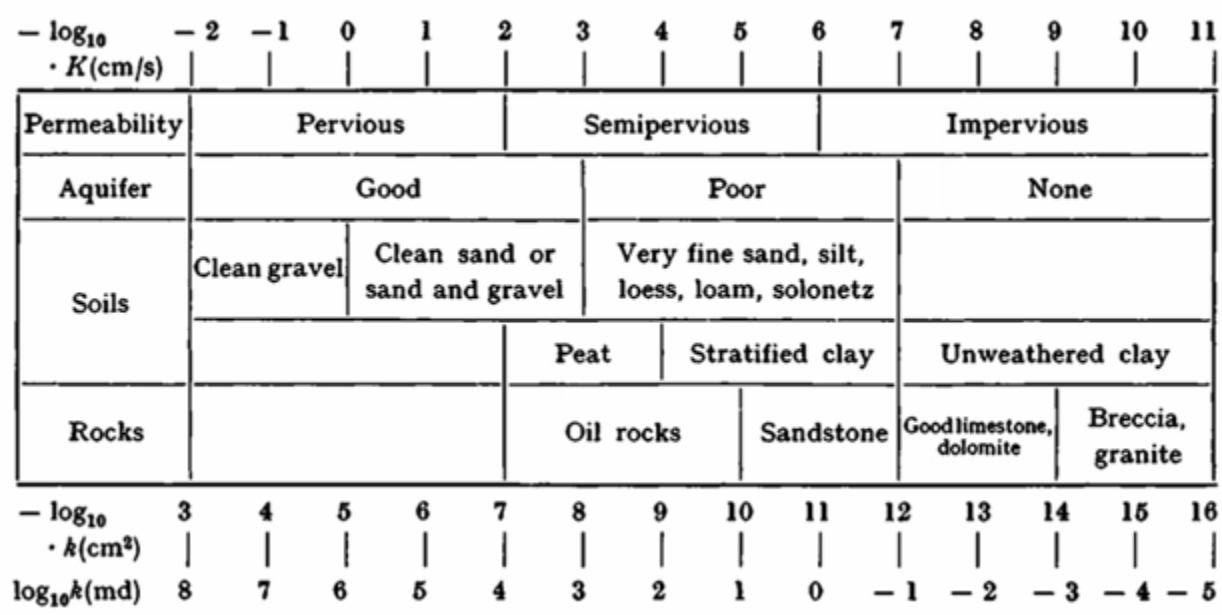

Figure 2.3: Typical Values of Hydraulic Conductivity and Permeability (Bear 1979).

2.1.4. Applications

Steady flow in porous media is relevant in assessing and evaluating solute transport within a given medium, concurrently involving chemical reactions between these transported substances and their surrounding environment, known as reactive transport. The study of reactive transport is quantitatively made using numerical modeling. However, establishing an experimental framework is essential to ensure better knowledge and understanding of the conceptual model of the reactive transport phenomena. (Khalil et al. 2022).

One example of these applications was presented by Hun et al. (2009), who evaluated the reactive transport of chemical elements in a Coastal Aquifer in Waquoit Bay, Massachusetts. The study's primary objective was to compare and analyze the total suspended concentrations of Fe (II) and As (III) in three distinct scenarios: field observations, laboratory experiments, and numerical modeling. In the modeling component, a two-dimensional (2D) simulation of the reactive transport of As in the discharging fresh groundwater was performed using the coupled MODFLOW 2005 and PHT3D models, which are widely recognized for their capabilities in simulating groundwater flow and solute transport processes, including reactive transport phenomena.

Other computational methods have been developed to compute reactive porous media flow. CrunchFlow (2019) is a software designed to model multicomponent reactive flow and transport phenomena. This tool simulates diverse physical processes within porous media, including diffusion, dispersion, and advection mechanisms. It is noticeable in the CrunchFlow manual (Steefel 2014) that the software does not primarily center on the hydraulic conductivity of porous

media but instead emphasizes the characterization of other pertinent hydraulic properties, such as resistivity, degree of saturation, and porosity.

Saaltink and Carrera (2004) conducted a comparative investigation on the computational performance of two prevalent mathematical methods employed for solving non-linear equations associated with reactive transport in groundwater: the Direct Substitution Approach (DSA) and the Sequential Iteration Approach (SIA). The study's outcomes revealed that DSA exhibited faster convergence and greater robustness than SIA. In a related study, Yeh and Tripathi (1989) state that the significant advantage of the SIA approach is the ability to use algorithms in cases where advection predominates over dispersion and diffusion, leading to a more readily achievable convergence.

Recently, Computational Fluid Dynamics (CFD) methods emerged as a valuable approach for investigating and understanding the complex phenomena of porous media flow for the microscale solution of the transport equations. Marcato et al. (2022) estimated porous media's permeability and filtration rate under laminar and steady flow conditions using neural networks, which are machine learning algorithms. Machine learning was integrated with a Computational Fluid Dynamics (CFD) simulation dataset to enhance the algorithm's accuracy. The investigation involved the creation of a porous media geometry, which employed a Gaussian particle size distribution to represent particle sizes. Notably, the results demonstrated an average error of less than 5%, attesting to the promising potential of using neural networks for permeability and filtration rate estimation in porous media analysis.

2.2. Transient Flows in Closed Pipe Flows

In addition to an understanding of porous media, knowledge about hydraulic transients assumes significance within the purview of this research, given its principal emphasis on the convergence of these topics. The following section present the pivotal ideas of this domain including the explication of transient phenomena, their practical implications, and the underlying governing equations.

2.2.1. Unsteady Flow Conditions

Unsteady flow in a closed-conduit system refers to conditions in which flow variables vary with time, such as flow rate, pressure, and velocity. The unsteady flow of liquids has been studied since the middle of the nineteenth Century (Freeze, 1994) and is of great importance in various engineering applications, such as pipe networks, open channels, and hydraulic structures. Understanding unsteady flow behavior in water conduits is crucial for predicting phenomena such as water hammer, pressure pulses, and wave propagation.

Water-hammer and transient flow are synonymously used to describe a well-known phenomenon associated with unsteady flow in conduits. It occurs due to sudden flow velocity or pressure changes, which propagate pressure waves through the system. According to Chaudhry (1987), the common causes of transients in hydraulics engineering systems are:

- Opening and closing of valves in a pipeline, either fully or partially.
- Starting or stopping the turbomachinery, such as pumps and turbines.
- The vibration of impellers or guide vanes in pumps.
- Sudden increases in the inflow to a river or a sewer due to stormwater runoff.

The study of pressure pulses is critical in Hydraulics Engineering to avoid failures related to the system's parts, including pipe ruptures, pump fatigues, and component damage. In the present work context, pressure pulses were generated at the upstream end of the apparatus, and the effects of these pulses on flows in porous media were subsequently investigated.

2.2.2. Governing equations and solution approaches for transient pipe flow

Wylie and Streeter (1978) state that the flow and pressure processes in transient conditions are governed by a PDE of motion, also known as momentum equation (Equation 2.7), and another PDE for mass conservation, or continuity equation (Equation 2.8). These equations can incorporate typical hydraulic components and their interactions with the conditions of the system, including boundary conditions.

$$\frac{\partial h}{\partial t} + \frac{a^2}{gA}\frac{\partial Q}{\partial x} = 0 \qquad 2.7$$

$$\frac{\partial h}{\partial x} + \left(\frac{1}{gA}\right)\frac{\partial Q}{\partial t} - f(Q) = 0 \qquad 2.8$$

In which H is the pressure head, Q is the volumetric flow rate, *a* is the pressure wave celerity, A is the cross-sectional area, g is the acceleration of gravity, and f(Q) is a pipe-resistance function. Those basic conservation laws consist of a hyperbolic PDE system solved within control volumes in conjunction with the boundary conditions describing specific time-varying flow conditions.

The concept of celerity or wave speed is related to the velocity as the pulse wave propagates in the pipeline once the transient period starts. In the absence of air fraction in conduits and for elastic pipe conditions, the celerity depends on the elasticity modulus of the fluid and pipe material, as stated in equation 2.9:

$$a = \frac{\sqrt{K_f/\rho}}{\sqrt{1 + c_1\left[\left(K_f/E\right)(D/e)\right]}} \qquad 2.9$$

Where K_f is the Elasticity Modulus of the fluid, E is Young's Modulus of Elasticity of the pipeline material, D is the Pipe Diameter, e is the pipe wall thickness, and c_1 is a constant that depends on the anchoring conditions of the pipeline. According to Wylie and Streeter (1978), the velocity of a pressure wave propagating within a fluid-filled pipeline can be significantly diminished due to gas bubbles, whether dissolved within the water or dispersed within the pores. When air is present in the pipeline, it becomes necessary to adjust the elasticity modulus of the fluid, denoted as K_m (Equation 2.10)

$$K_m = \frac{\mu_f}{1 + \left(V_g/V_f\right)\left(\frac{\mu_f}{\mu_g} - 1\right)} \qquad 2.10$$

Where V_l and V_g are the total volume of liquid and gas, respectively, and K_g is the modulus of elasticity of the gas. When pipe wall materials are not elastic, further adjustments are needed to describe transient pipe flows. Studies developed by Soares et al. (2008) analyzed transient flows in polyvinyl chloride (PVC) pipes. The creep function that describes the viscoelastic rheological characteristics of PVC was obtained through data collection from an experimental system comprising a series of PVC pipes. Additionally, an inverse transient model was developed, accounting for the viscoelastic properties of the material.

Martins et al. (2016) created a Computational Fluid Dynamics (CFD) model to analyze hydraulic transient flows in pressurized systems. The model incorporates a three-dimensional mesh developed in a prior study by Martins et al. (2014). Experimental data were collected from an unsteady pipe system to assess the model's accuracy and reliability, providing valuable validation for the CFD simulations. This research explored two distinct valve opening scenarios:

instantaneous and time-function valve opening. The findings consistently characterized the pressure wave's shape, adhering to the governing hyperbolic PDEs presented above.

2.3. Transient Flow in Porous Media

The last literature review subchapter shows the main equations that govern the hydraulic transient in porous media, including the boundary conditions for those formulations.

2.3.1. Governing Equations

The determination of the piezometric head at any given time and location within a hydraulic system can be achieved through the solution of a parabolic partial differential equation. The one-dimensional version of this equation, as proposed by ye e in 1966, represents an adapted form of the diffusion equation.

$$\frac{\partial H}{\partial t} - \left(\frac{K}{S_S}\right)\frac{\partial^2 H}{\partial x^2} = 0 \qquad 2.11$$

Where h is the water head function, and S_s is the specific storage of the porous media. In work conducted by Ye et al. (2021), an analytical solution was presented for assessing the piezometric head at any given point and time within an unsteady flow system in a semi-infinite porous media. In this scenario, the water head is constant and equal to H_1 in the upstream point of the system and $h_0$in all other points. The solution is presented below:

$$H(\mathrm{x,t})|_{t=0} = \mathrm{H_0} \qquad 2.12$$

$$H(\mathrm{x,t})|_{x=0} = \mathrm{H_1} \qquad 2.13$$

$$H(\mathrm{x,t})|_{t=\infty} = \mathrm{H_0} \qquad 2.14$$

$$H(\mathrm{x,t}) = \mathrm{H_0} + (H_1 - \mathrm{H_0}) * erfc\left(\frac{x}{2\sqrt{K\bar{H}\mathrm{t}/\mu}}\right) \qquad 2.15$$

Where K is the hydraulic conductivity of the porous media material, μ is the specific yield of the porous media material, and $\overline{h} = \frac{H_0+H_1}{2}$. The variables "x" and "t" represent the position and time for the corresponding head to be determined. *erfc* represents the error function defined as

$$erfc\ x = \frac{2}{\sqrt{\pi}} \int_x^{\infty} e^{-t^2} dt \qquad 2.16$$

Equation 2.11 applies equally to a finite porous media domain comprising a reservoir, a pipeline filled with porous media, and an interposed valve. However, this scenario employs the Neumann boundary condition as a key distinction. Under the Neumann boundary condition, the derivative of the dependent variable is regarded as constant (Mazumder, 2015). Equation 2.17 illustrates the specific boundary condition utilized in this type of system.

$$H'(L,t) = 0 \qquad 2.12$$

Where x=L represents the downstream end of the system. The apostrophe means that H' is the first derivative of the function H.

As demonstrated in the preceding chapter, extensive research has been conducted to investigate porous media, its properties, and the steady flow characteristics within such media. Furthermore, numerous studies have examined hydraulic transients in closed conduit pipes. Concerning the integrated investigation of porous media and hydraulic transient phenomena, the primary studies in the literature are related to theoretical studies and numerical models. However, very few studies experimentally approach the phenomena of hydraulic transients in porous media and the influence of the media's hydraulic conductivity on the behavior of the pressure wave, reinforcing the relevance of the present research.

3. Methodology

This chapter describes the experimental model constructed in the Water Resources Laboratory at Auburn University. The methodology is structured into three parts:

- Experimental setup and description section: Includes the essential elements of the hydraulic system, geometric parameters governing the system, detailed material descriptions and associated properties, specifications of the data acquisition instruments employed, and calibration procedures.
- Standardized tests section: Provides details of the sieving tests, which served a dual purpose: firstly, to ascertain material granulometry, and secondly, to effectively segregate materials into distinct diameter ranges. Moreover, an adapted permeameter test is presented in which the experimental model serves as a reliable constant head permeameter, making it possible to precisely determine the hydraulic conductivity of all materials used in this study.
- Data acquisition procedure section: Describes a step-by-step of the data acquisition process conducted during transient flow tests. It encompasses key details such as apparatus preparation, experimental time frame, frequency of data acquisition, and subsequent data post-processing procedures.

3.1. Experimental Setup and Description

The fundamental components of the experimental apparatus used in this investigation consisted of a water reservoir, an interconnected transparent pipe, and a solenoid valve between the pipes and the reservoir. Additional ball valves were introduced to the system to enable flow

control and address boundary conditions for experimental purposes. Figure 3.1 shows a profile view schematic of the experimental apparatus.

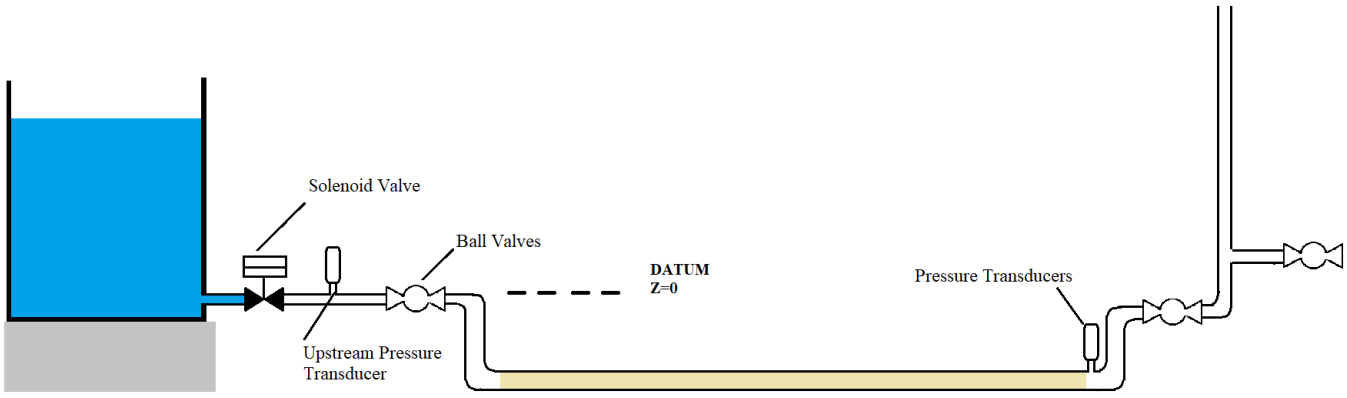

Figure 3.1: Profile view of the apparatus:

As noticeable in Figure 3.1, the axis of the main pipeline segment exhibits a slight offset, positioning it below the level of the water tank's base. This arrangement was implemented to generate a favorable positive pressure in the given section, thereby mitigating the admission of external air into the system.

The solenoid valve is an essential system component due to its fast action to pressurize the system within a few milliseconds. This rapid opening mechanism is critical as it facilitates the prompt initiation of transient flows, minimizing undesirable interferences caused by manual openings that may be inherently slower. Four parallel and interconnected pipeline segments were linked to the upstream reservoir and solenoid valve to enable simultaneous testing of various porous media under equal conditions. An upstream pressure transducer was placed at the derivation's upstream end, leading to the separated pipe segments. Figure *3.2* presents a top view of the experimental apparatus, showing the parallel arrangement of the four conduits. Figure 6 presents the upstream end of the apparatus, and Figure 3.3 indicates different types of porous media in the pipe segments.

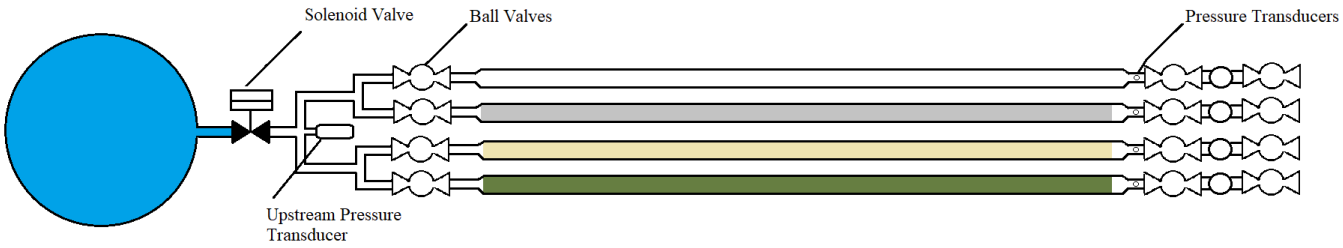

Figure 3.2.: Top view of the apparatus.

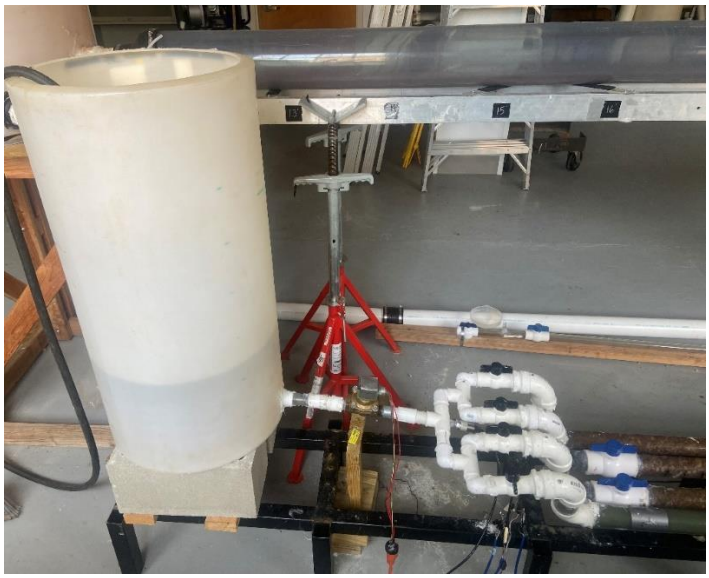

Figure 3.3: Upstream section of the apparatus

Figure 3.4: Downstream section of the apparatus

As shown in Figure 7, Each pipe segment was fitted with different media (i.e., porous media or water), one pressure transducer, and three ball valves that enabled isolation of the segment and different types of downstream boundary conditions. In addition to the solenoid valve, three additional valves, specifically ball valves, were incorporated within the system. The upstream ball valve was used as an isolation valve and was closed if a pipe segment was not tested in a given experimental run. The other two ball valves were positioned at the downstream end of the segments and enabled three conditions at the downstream end. Using Figure 3.1 as a reference, these conditions were:

- Capped outlet: When the two downstream ball valves were closed, also called *Cap Tests*. No outflow was allowed, and pressure waves from the upstream tank would reach and potentially bounce off the ball valve.
- Open to the atmosphere with no outflow: The first downstream ball valve was opened, but the second valve was closed. Such conditions are also called *Surge Tests*, enabling water to rise through a vertical segment, but no outflow occurs.
- *Free outflow tests*: When the two ball valves were open, there was free discharge from the apparatus.

Tables 1 and 2 present the geometric characteristics of the principal constituents of the system, along with their respective elevations relative to the datum. It is conventionally recognized that the datum of the system corresponds to the elevation of the downstream pressure transducers, denoted as z=0 at those specific locations, as illustrated in Figure 3.1.

Table 3.1: Geometric parameters of the system

Water Tank	
Diameter	51.0 cm (20.1 in)
Height	97.0 cm (38.2 in)
Pipelines	
Diameter	5.0 cm (2.0 in)
Length	228.0 cm (89.8 in)

Table 3.2: Elevation of the main components of the system above the datum

Component	**Elevation (cm)**
Water Tank Bottom	1.0
Water Tank Orifice	4.5
Solenoid Valve	4.5
Upstream Pressure Transducer	0
Downstream Pressure Transducers	-17.5
Discharge Valve	-1.5
Pipeline Bottom	-22.5

Upon the completion of interconnecting all apparatus components, it was essential to apply caulk to the junctions and discontinuities of the system. This step aimed to prevent any possible leakage during the experimental procedures. The application of caulk was conducted systematically following the subsequent procedural steps: initially, all valves were opened, then identifying and marking areas exhibiting leakage. Subsequently, the solenoid valve was closed, and observation was undertaken until the cessation of water dripping. After this observation period, caulk was applied to the identified leaking points, allowing for a designated drying duration of 24 hours. This process was iteratively repeated across all sections of the experimental model until any remaining leakage points were eliminated.

Furthermore, holes were drilled in the PVC pipe to serve as ventilation points at various points along the pipeline segments to facilitate the elimination of trapped air within the system. This precautionary measure was implemented to minimize the influence of air in the experiments, which would influence the dynamics of pressure propagation. However, while most air was eliminated, it was sometimes observed that some residual air phase was still present within the porous media during the tests.

Lastly, in order to create conditions that better approach the apparatus from ideal test conditions, it was necessary to anchor the pipelines. Those conditions were achieved using steel wires wound around the pipelines and pliers tightening them. As an additional measure, weights (e.g., 50-pound cement bags) were placed over the pipe segments to reduce the motion within the apparatus during the tests. These weights helped to reduce signal noises in the output data created by vibrations or motion in the apparatus.

3.2. Description of the tested Porous Media

The present study aimed to assess transient flows of various porous media materials, and to achieve this objective, a decision was made to conduct two distinct series of experiments. Each series involved the utilization of diverse porous media materials. The subsequent subchapters will describe each specific porous media material employed in this research, elucidating their characteristics and properties.

The sand in these tests consisted of the finest porous media used in this research. Given that the particle size of the material is not uniform, the process of sieving is necessary to characterize the material properly. Thus, a sieving test was performed following the ASTM E11 standard. In order to characterize the sand, a set of four distinct sieve sizes was employed, namely: 500 μm

(#35), 250 µm (#60), 106 µm (#140), and 53 µm (#270). The findings indicate that 3.5% of the sand mass was retained in sieve #60, 81.3% in sieve #140, and 15.2% of the mass was retained in sieve #270. Only a negligible quantity of the material was retained in the sieve of 500 µm. Hence the amount of material that stayed in that sieve can be considered virtually equal to zero. shows the particle size distribution of the sand used in this research. The percentages represent the amount of finer material by weight.

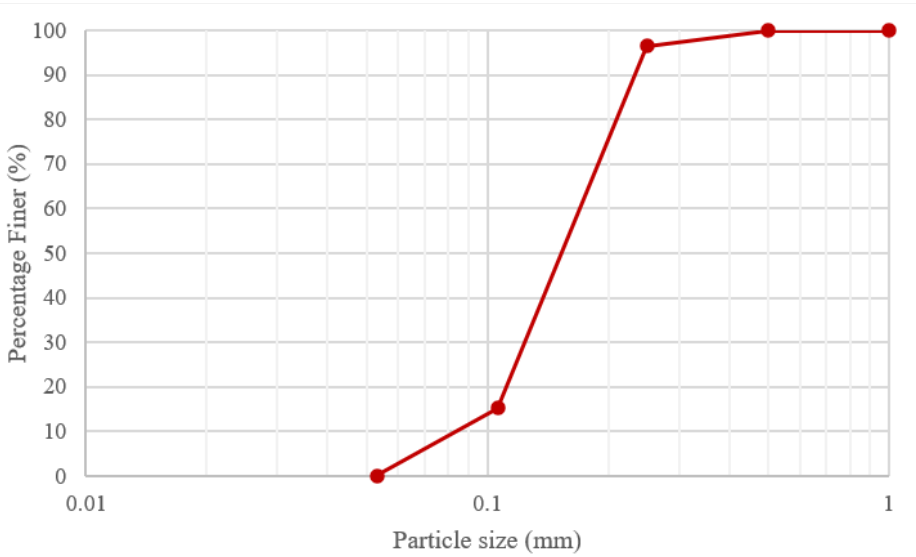

Figure 3.5: Particle size distribution of the sand media used in the transient pressure pulse tests.

Glass beads of two different diameter sizes were used: 1.0 mm and 15.0 mm. We assumed that both materials have a uniform size distribution, meaning that all particles have approximately the same diameter.

The Pea pebbles in this study exhibited a relatively wide range of particle diameters. Therefore, it was necessary to separate the particles into different diameter ranges. Considering the objective of achieving an intermediate diameter falling between 1 and 15 mm, a series of sieves were employed, each possessing a diameter within this specified range. Specifically, sieves with diameters of 2.0 mm (#10), 4.7 mm (#4), 8.0 mm (5/16 in), and 9.5 mm (3/8 in) were

utilized in the experiment. These sieves separated the Pea pebble material into pipe segments: 2.0 to 4.7 mm, 4.7 to 8.0 mm, and 8.0 to 9.5 mm. The following figure details all the porous media materials employed in this research.

Figure 3.6: Tested porous media materials.

3.2.1. Experimental Series

Two series of experiments were performed in this research, with the first involving a broad particle size range, from sand to 15-mm diameter glass beads. The second series of experiments used a narrower range of particle sizes, focusing on pea pebbles, as is shown in Table 3.3. All tested media was previously saturated with water prior to testing.

Table 3.3: Series of porous media tested during the experiments.

Series	**Pipe segment 1**	**Pipe segment 2**	**Pipe segment 3**	**Pipe segment 4**
1	Glass Beads (1 mm)	Glass Beads (15 mm)	Sand	Water (No porous media)
2	Not used.	Pea Pebbles (4.7 to 8.0 mm)	Pea Pebbles (8.0 to 9.5 mm)	Pea Pebbles (2.0 to 4.7 mm)

It is essential to highlight that, despite an adequate quantity of material to fill pipelines 3 and 4, the availability of pea pebbles within the 2.0 mm to 4.7 mm range fell short of completely filling pipeline 2. For that reason, a decision was made to combine the available media with pea pebbles of the next larger diameter (4.7 to 8 mm) in a volumetric ratio of 3:1. The resulting blend consisted of 75% pea pebbles within the 2.0 mm to 4.7 mm range complemented by 25% material ranging from 4.7 mm to 8.0 mm. This blending approach ensured enough material to achieve the apparatus's needed porous media volume. Figure 3.7 presents the apparatus with the different types of porous media installed.

(a)

(b)

Figure 3.7: Series 1 (a) and 2 (b) of experiments

3.3. Measurement instrumentation

The instrumentation deployed in the research aimed to gather high-frequency pressure data from the system. The instrumentation primarily comprised a data acquisition board connected with multiple pressure transducers strategically positioned at various locations within the apparatus. Furthermore, these pressure transducers were linked to a dedicated power supply source, ensuring a reliable and unwavering constant voltage input for seamless data acquisition and recording.

A data acquisition board was used to acquire and process analog or digital signals from various pressure transducers installed in the apparatus. In this research, pressure transducers are connected to the data acquisition board, providing analogic voltage signals that are subsequently processed by the Data Acquisition Board (DAQ). The entirety of the acquired data is saved and stored on a computer directly linked to the board, and the pressure signals need to be converted to pressures subsequently through a calibration procedure. The data acquisition board employed in this study is the National Instruments USB-6210 model, which can process 250,000 signals per second, thus suitable for capturing high-frequency data (i.e., kHz range) in the experimental setup. Up to eight pressure transducers can be used in the board, but only four were used in the experiments. The Data Acquisition (DAQ) device was connected to a computer through a USB cable, establishing an interface for data transmission. The data processing and retrieval tasks were performed using the National Instruments DAQExpress software, which enabled the results to be exported to a CSV file for subsequent analysis.

The pressure transducer needs to be connected to a dependable source of constant voltage, as the quality of the output voltage signal depends on the input voltage. The direct current regulated power supply VOLTEQ HY3003DX was employed for this purpose. This device can generate a

constant current ranging from 0 to 3 Amperes or a constant voltage from 0 to 30 Volts. The power supply is equipped with coarse and fine controls for setting the voltage and current outputs. This functionality enables accurate calibration and adjustment of the supplied voltage of the transducer.

The pressure transducer employed in the experimental setup is the General Electric UNIK 5000 model. The model used has a measurable pressure range from -2.00 psi (-13.81 kPa) to 2.00 psi (13.81 kPa), allowing for the accurate measurement of both negative pressures and pressures up to 100% higher than the initial piezometric head of the system (1 psi). The sensor supply voltage range associated with this pressure transducer is from 2.5V to 12V, and the recommended fixed supply voltage is equal to 10 V. The accuracy of these transducers is 0.1% of the full scale or $\pm$14 Pa.

A polyurethane cable connects the power supply and data acquisition board to the pressure transducer. This cable consists of six individual wires with specific functions and colors: red wire for positive supply, white wire for negative supply, yellow wire for positive output, blue wire for negative output, orange wire for shunt calibration, and a bare wire for ground connection. provides a schematic draft illustrating the equipment connections.

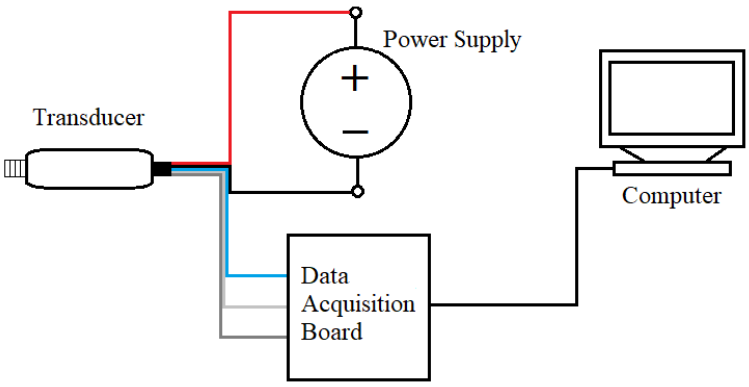

Figure 3.8: Schematic draft of the equipment connections

3.4. Hydraulic conductivity of the tested porous media

A component of this research was assessing and characterizing hydraulic conductivity for the different porous media employed during the experimental investigation. This evaluation was performed by applying fundamental principles derived from Darcy's Law in conjunction with a modified implementation of the conventional permeameter test under constant head conditions. The modified permeameter test employs the apparatus as a form of permeameter, wherein the reservoir serves as the source of a constant head, and each pipeline segment functions analogously to a cylindrical column of soil in the permeameter setup.

The methodology employed for determining hydraulic conductivity exhibited a relatively straightforward nature. The procedure involved opening the solenoid valve and all the globe valves within the pertinent pipeline. Subsequently, a brief period was allotted for establishing a stabilized flow state, whereby a receptacle was positioned at the outlet of each pipe segment to capture the discharged water from each tested porous media. The duration of the tests was set to 60 seconds, except for the sand media, which lasted for 17 minutes, and the time measurement accuracy was estimated at 0.5 seconds. The mass of water was subsequently measured, and the weight difference and experiment duration enabled the inference of the flow rate yielded by each porous media in the pipe segments. It was assumed that the water density at room temperature and the experimental pressure conditions (atmospheric pressure) was 0.998g/cm^3 (Haynes 2014).

Once the flow rate of each porous media was determined, it was possible also to determine the flow velocity, dividing the flow rate by the effective cross-sectional area. Using this velocity (V), combined with other parameters, namely, water density (ρ), water dynamic viscosity (μ) and

characteristic diameter (D, considered to be equal to the predominant diameter size of the porous media), it was possible to determine the Reynolds Number of all porous media flow, as shown in the following equation:

$$Re = \frac{\rho V D}{\mu} \qquad 3.1$$

3.5. Pressure Transducers calibration

Since the piezometric transducer output obtained through the data acquisition is given in voltage, it was necessary to establish a calibration curve for the conversion into corresponding pressure values. It is known that the voltage output in such transducers varies linearly with the pressure, thereby establishing a function to describe the association between pressure and voltage.

The procedure of determination of the calibration curve entailed the execution of the following steps: 1) data collection was initiated with the acquisition board and DAQExpress software; 2) each pressure transducer was immersed in the upstream reservoir, ensuring that the initial water level was 63.5 cm. Subsequently, a systematic reduction in water level was implemented at 12.7 centimeters intervals, progressing towards the ultimate target level of 12.7 centimeters (five inches). Then, the recording was interrupted, and the data were saved and imported to Microsoft Excel. Each distinct water depth measurement was systematically associated with its corresponding transducer voltage output, establishing the linkage between voltage and pressure, thus enabling the calibration curves presented in Table 3.4 and Figure 3.9.

Table 3.4: Voltage-pressure relation of each pressure transducer

Sensor number	Calibration Function
Sensor 1	$P = \frac{V - 18.387}{0.2622}$
Sensor 2	$P = \frac{V - 37.170}{0.2585}$
Sensor 3	$P = \frac{V - 38.479}{0.2579}$
Sensor 4	$P = \frac{V - 39.218}{0.2593}$

Where V is the voltage in millivolts and P is the pressure in centimeters of water.

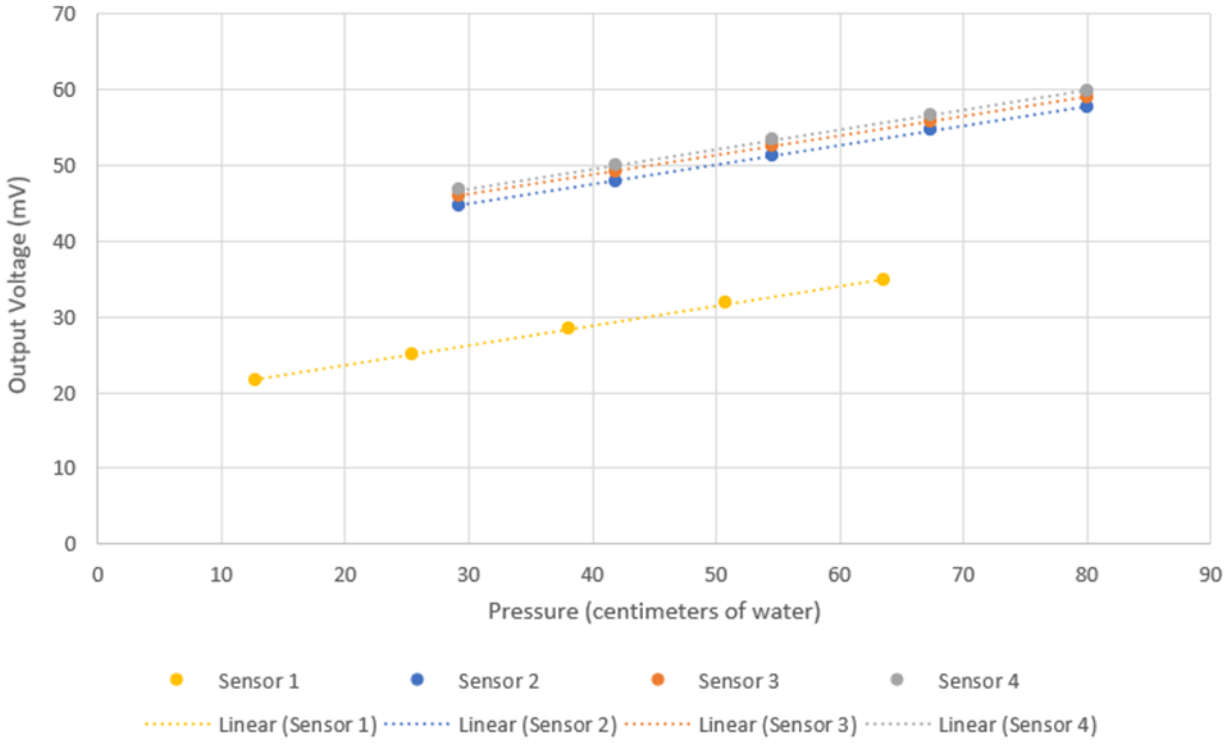

Figure 3.9: Calibration curves for the pressure transducers used in the experiments.

3.6. Experimental procedure

To minimize human interference, standardized procedures were established for data acquisition during unsteady flow experiments. Consistent steps were employed across all tests,

ensuring uniformity, with only specific deviations in simulation time and data acquisition frequency due to the unique characteristics of each test. These measures were implemented to enhance the reliability and comparability of the acquired data, thereby facilitating accurate analysis and interpretation of the unsteady flow phenomena under investigation.

1) The tank was filled with water until it reached a specific height of 70.3 centimeters (27.7 inches). This water level was chosen to establish an initial piezometric head of 1 psi ($6.9*10^3$ Pascal) at the base of the reservoir. It was assumed that the water level within the tank remained constant throughout the experiment's entire duration in the tests involving water discharge. This assumption stemmed from the fact that the flow rate was considerably low, not being sufficient to cause a substantial reduction in the water level within the tank.

2) Once the reservoir was filled to the desired level, the air was eliminated from the apparatus through the air discharge points at various points. The air discharge locations were subsequently sealed to prevent air intrusion and water leakage.

3) Then, the power supply was activated, and the voltage was adjusted to a precise value of 10.00V, following the transducer's prescribed recommendation.

4) The data acquisition frequency was subsequently adjusted within DAQ SignalExpress. This frequency was contingent upon the specific test and the characteristics of the porous media under investigation. For instance, in the case of materials with relatively low permeability (i.e., sand), the transient period was longer, necessitating a lower data acquisition frequency so that the data collection was manageable. Conversely, conditions such as the Free Flow test with higher permeable media had rapid response times and

shorter transient durations, requiring a higher data acquisition frequency. shows the adopted frequency range for each type of test.

Table 3.5: Frequency Range for each type of test

Test Name	**Frequency Range**
Cap Test	10 Hz to 10000 Hz
Surge Test	500 Hz to 2000 Hz
Free Flow Test	2000 Hz to 5000Hz

5) The solenoid valve was then closed, and pressures at the downstream end of the apparatus were reduced by opening the downstream ball valves. Thus, The solenoid valve separated the apparatus's high-pressure region (i.e., reservoir) from the low-pressure region (i.e., pipe segments).

6) The experimental data started to be recorded in the DAQ SignalExpress, and then the solenoid valve was opened, initiating the transient flow conditions.

7) The data collection continued for a predetermined duration (specifically 3 seconds), after which the solenoid valve was closed. The data collection varied from 10 seconds for Cap Tests to 20-30 seconds for Surge and Free Flow Tests. In the cases in which sand was used, the duration of the data collection was longer, and the frequency of pressure data collected was decreased.

8) After the data recording process was terminated, the exported CSV files were imported to Excel and subjected to data processing procedures, converting voltage into pressure data

using the data calibration curves. A simple numerical filter was applied to the data by averaging a time value for voltage over various adjacent voltage readings to reduce noise, not impacting the representation of pressure pulses, as indicated in Figure 3.10.

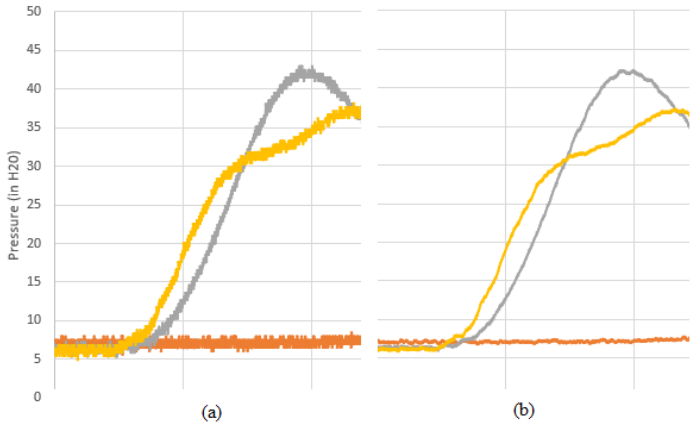

Figure 3.10: Example of pre-filtering (a) and post-filtering (b) graph

3.7. Numerical Method

A numerical Model was developed to compare and validate the experimental outcomes. It was made by using Excel functions in conjunction with the VBA programming language. Specifically, two distinct models were constructed: the first model was dedicated to simulate surge tests, predicated upon the foundational principles of Darcy's Law, while the second model pertained to capped tests and was grounded in the parabolic partial differential equation.

3.7.1. Numerical Schemes

Cap Tests

For the capped test, the numerical scheme that was implemented was the forward-time-centered space (FTCS). So, the parabolic PDE (Equation 2.11) can be discretized as following:

$$\frac{H_i^{n+1} - H_i^n}{\Delta t} = (\frac{K}{S_s}) \frac{H_{i+1}^n - 2H_i^n + H_{i-1}^n}{\Delta x^2}$$

$$\frac{H_i^{n+1} - H_i^n}{\Delta t} = \left(\frac{K}{S_s}\right) * \frac{H_{i+1}^n - H_i^n}{\Delta x^2} + \left(\frac{K}{S_s}\right) * \frac{H_{i-1}^n - H_i^n}{\Delta x^2}$$

Where n is the current time, i is the discretized node, Δt is the time step, Δx is the space step.

Boundary Condition at the downstream end.

The downstream Boundary Condition used was the Neumann BC, which states that the derivative of the function H over space is equal to zero in the downstream end of the hydraulic system, as shown below:

$$\frac{\partial H}{\partial x} = 0$$

$$\frac{H_{i+1} - H_i}{\Delta x} = 0$$

Combining the FTCS with equation above, it is possible to find the iterative equation for the downstream end of the system.

$$\frac{H_i^{n+1} - H_i^n}{\Delta t} = \propto \frac{H_{i-1}^n - H_i^n}{\Delta x^2}$$

The head at the iteration n+1 is hence calculated as:

$$H_i^{n+1} = H_i^n + \frac{\propto * \Delta t}{\Delta x^2} (H_{i-1}^n - H_i^n)$$

Surge Test

$$Q = -kA\frac{dH}{dL}$$

$$Q = \frac{k * A_p * (H_u - H)}{L_p}$$

Replacing Q as the first derivative of volume over time:

$$\frac{dV}{dt} = \frac{k * A_p * (H_u - H)}{L_p}$$

$$A_v\frac{dH}{dt} = \frac{k * A_p * (H_u - H)}{L_p}$$

Discretizing the equation using Forward Euler equation:

$$A_v\frac{\Delta H}{\Delta t} = \frac{k * A_p * (H_u - H)}{L_p}$$

$$\Delta H = \frac{\Delta t * k * A_p * (H_u - Hs)}{A_v * L_p}$$

$$H^{n+1} - H^n -= \frac{\Delta t * k * A_p}{A_v * L_p} * (H_u - H^n)$$

Isolating the H^{n+1} term:

$$H^{n+1} = H^n + \frac{\Delta t * k * A_p}{A_v * L_p} * (H_u - H^n)$$

4. Results and Discussion

4.1. Pressure signal results

As pointed out in the Literature Review, the closed-pipe transient flows are governed by a hyperbolic Partial Differential Equation (PDE), with the simplest example being the wave equation. The solution of such equations is characterized by the space-time translation of flow features, such as pressure waves, over the solution domain. As a result, a pressure pulse originating at the upstream end has features identifiable at a location downstream after some time. On the other hand, transient flows in porous media are dominated by energy losses, and the response of sudden pressure changes at one boundary is typically a gradual pressure rise in the solution domain. Such an increase can be described by the parabolic partial differential equation presented in the Literature review. The representation of the pressure responses when the tested apparatus was capped at the downstream end in Figure 4.1 provides a contrast between the typical hyperbolic and parabolic responses for a sudden upstream pressure rise.

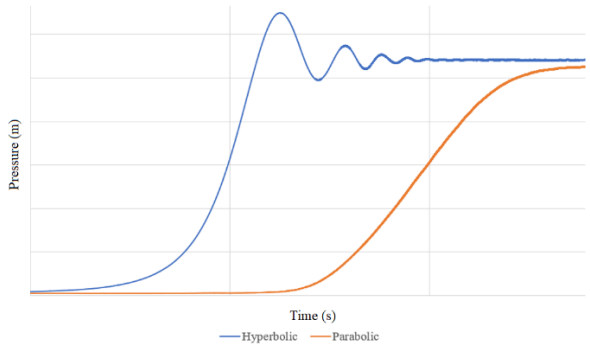

Figure 4.1: Typical pressure responses for hyperbolic and parabolic PDE behaviors for one capped experiment, with the time axis in the log scale.

As is noticeable in Figure 4.1, hyperbolic-type results exhibit recurring pressure peaks and rapid pressure growth. Notably, the magnitude of the peak pressure often exceeds the steady-

state pressure, showing the key differences in pressure pulse reflections, as mentioned in the Literature Review. Due to energy dissipation, the pressure peak amplitudes gradually diminish with each successive cycle, approaching values closer to the steady-flow level. This phenomenon is explained by energy dissipation during each wave reflection, attributed to imperfections in the anchoring, friction losses, and elastoplastic properties of the PVC pipeline (Chaudhry 1987).

On the other hand, the parabolic curve does not display peak pressures in the initial moments after the beginning of transient flows; instead, the pressure undergoes a slow and gradual increment until it reaches the steady-state level. The curve is expected to conform to the format of the error function curve.

4.2. Consistency of the pressure measurements

Following the methodology outlined in Section 3.6, each type of test was repeated five times to assess the consistency of data acquisition and verify the absence of significant variability between repetitions. This approach ensures the reliability and robustness of the obtained results. Figure 4.2 exhibits the results of the pipe filled with water only in the Capped tests. The observation reveals a substantial overlap among all five curves, indicating minimal variability in the results. Consequently, for brevity and to maintain clarity, the subsequent presentation of results will include only one of the five performed repetitions, as it serves as a representative example that accurately represents the consistency across all repetitions.

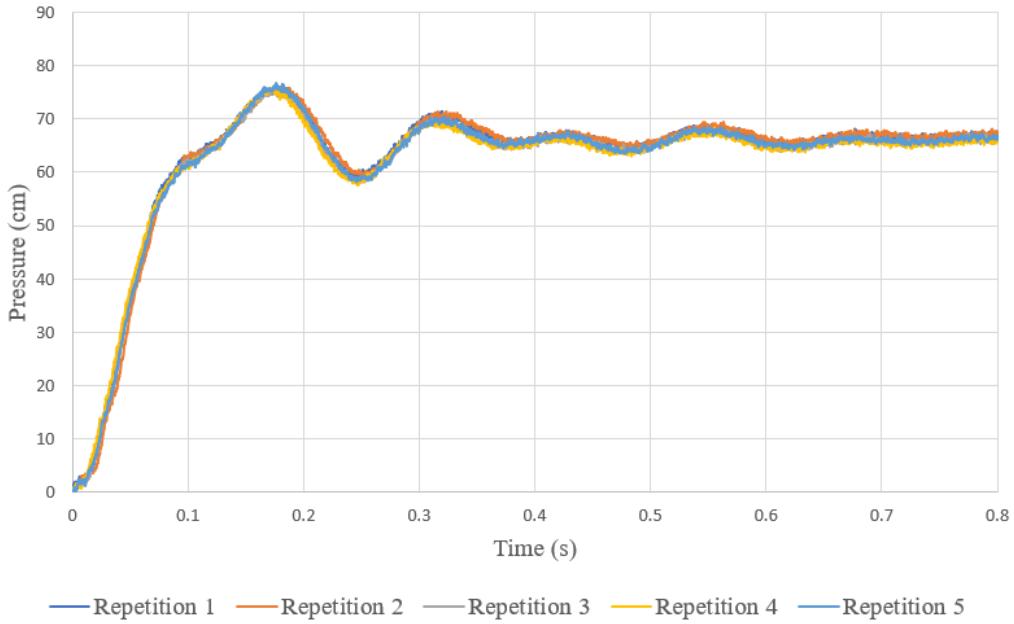

Figure 4.2: Graph that illustrates the repetitions for the water conduit in the Capped test.

4.3. Flow Characteristics

Table 4.1 presents the Reynolds Number and the requisite parameters in its computation. Notice that the characteristic length was assumed to be equivalent to the average diameter within the respective range for pea pebbles. In contrast, it is equal to the predominant diameter of the granulometric distribution for the sand and equal to the characteristic diameter of the glass beads, whose granulometry was assumed as uniform.

Akan (2006) states that the water flow can be categorized as laminar when its Reynolds Number is below 2000, transitional when the Reynolds Number falls between 2000 and 5000, and turbulent for values exceeding 5000. Table 4.1 indicates that all flows tested in the various porous media have Reynolds below the laminar flow threshold. The relevance of this observation lies in its validation of the utilization of Darcy's Law, which assumes the flow to be within the laminar regime (Bear 1979). The total water volume collected in the adapted permeameter test, its respective experiment time, and the hydraulic conductivity are presented in Table 4.2.

Table 4.1: Reynolds Number values for the tested conditions.

Material	**Flow Rate (**m^3/s**)**	**Flow Velocity** (cm/s)	**Characteristic dimension** (mm)	**Reynolds Number** (dimensionless)
Sand	$1.96*10^{-8}$	$9.69*10^{-4}$	0.106	$1.77*10^{-3}$
Glass Beads (1 mm)	$6.93*10^{-6}$	0.34	1.00	$5.89*10^{0}$
Pea Pebbles (2.0 to 4.7 mm)	$3.79*10^{-5}$	1.87	3.35	$1.08*10^{2}$
Pea Pebbles (4.7 to 8.0 mm)	$4.72*10^{-5}$	2.33	6.35	$2.55*10^{2}$
Pea Pebbles (8.0 to 9.5 mm)	$7.16*10^{-5}$	3.53	8.75	$5.32*10^{2}$
Glass Beads (15 mm)	$1.48*10^{-4}$	7.30	15.00	$1.89*10^{3}$

Table 4.2: Hydraulic conductivity parameters

Material	**Experiment Time (s)**	**Water Volume (ml)**	**Hydraulic Conductivity (m/s)**
Sand	10260	201.5	$3.74*10^{-5}$
Glass Beads (1 mm)	60	415.5	$1.24*10^{-2}$
Pea Pebbles (2.0 to 4.7 mm)	60	2272.0	$5.91* 10^{-2}$
Pea Pebbles (4.7 to 8.0 mm)	60	2832.0	$7.37 *10^{-2}$
Pea Pebbles (8.0 to 9.5 mm)	60	4293.0	$1.11* 10^{-1}$
Glass Beads (15 mm)	60	8875.5	$2.64*10^{-1}$

To ensure that the water tank level is remained approximately constant during the hydraulic conductivity determination, it is necessary to assess the fluctuation in water levels. This evaluation is conducted in the scenario characterized by the maximal flow rate, denoted by the utilization of glass beads with a diameter of 15 mm. Considering the experiment time equal to 60 seconds and a flow rate equal to $1.48*10^{-4}$ m^3/s, the total discharged water volume is $8.88*10^{-3}$ m^3/s, which is capable to decrease the water tank level in 0.043 m. Hence, even considering the critical scenario, the water level variation is not superior to 6.15% of the initial tank level.

The hydraulic conductivity of all tested porous media ranged from 10^{-1} to 10^{-2} m/s, except for the sand, whose conductivity was in the order of magnitude of 10^{-5} meters per second. These

values are consistent with other sources of hydraulic conductivity in porous media (Bear 1979). The data presented in the table reveals that the primary factor governing this property is the characteristic dimension. Notably, the hydraulic conductivity diminishes as the diameter of the material decreases. This finding aligns with the anticipated outcome, as a smaller material diameter typically reduces the average pore size. Consequently, water experiences more energy losses during flow, leading to a reduction in the flow rate.

4.4. Capped tests: experimental results

The Capped tests corresponded to the situation where the downstream end of the pipe segments was closed entirely, and no flow occurred. Pressure results shown in Figure 4.3 indicate that larger porous media diameters and the case with only water in the pipeline showed periodical pressure peaks, typical of transient flows described by hyperbolic PDEs. By contrast, the two smallest tested porous media, sand, and 1-mm glass beads indicated a gradual pressure growth, typical behavior of more traditional porous media transient flows.

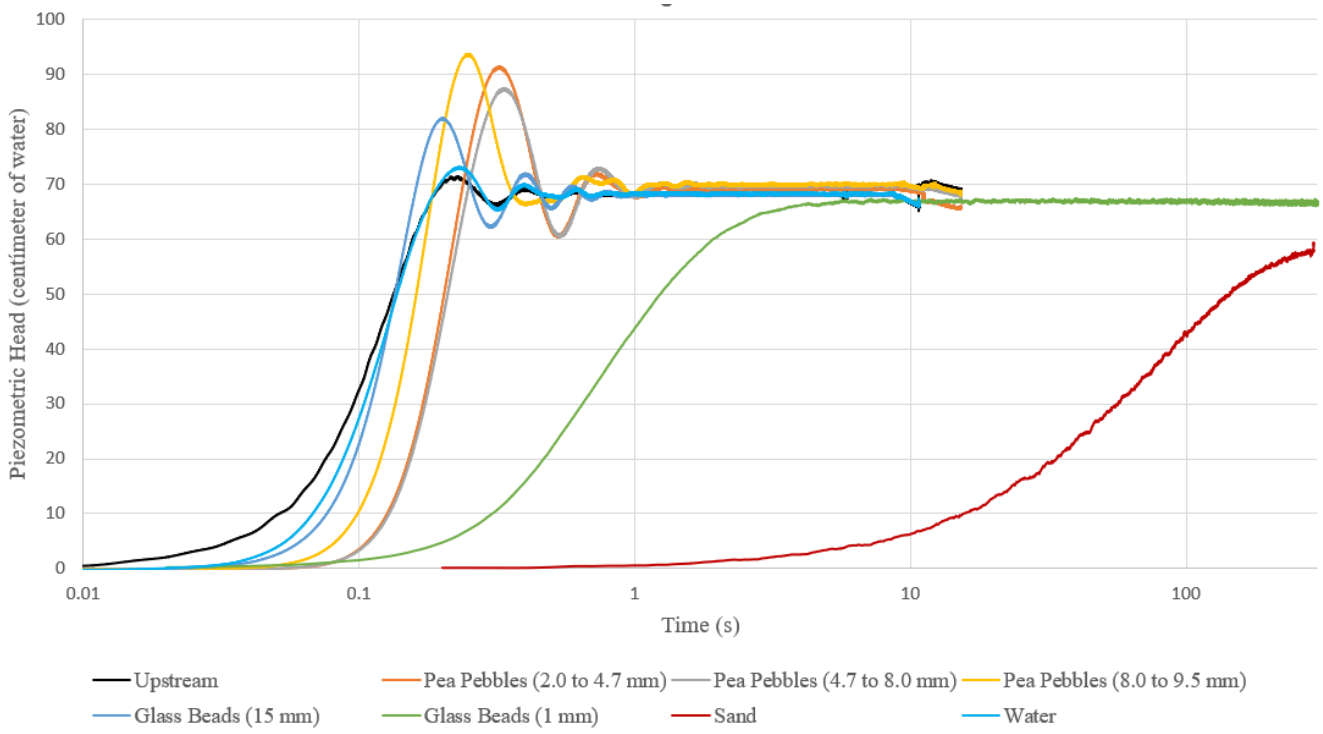

Figure 4.3: Piezometric Head over Time for the capped experiments.

A criterion was selected to determine the arrival of a pressure disturbance generated at the downstream end of the pipeline segments. The arrival time was selected when the downstream transducer detected an increment above 0.1% of the steady flow pressure head, which was the error threshold of the pressure transducer. Figure 4.4 presents the measured time, including the experimental variability, when the downstream pressure transducers detected the arrival of the pressure pulse. The vertical axis, in logarithmic scale, represents the pressure arrival time in milliseconds.

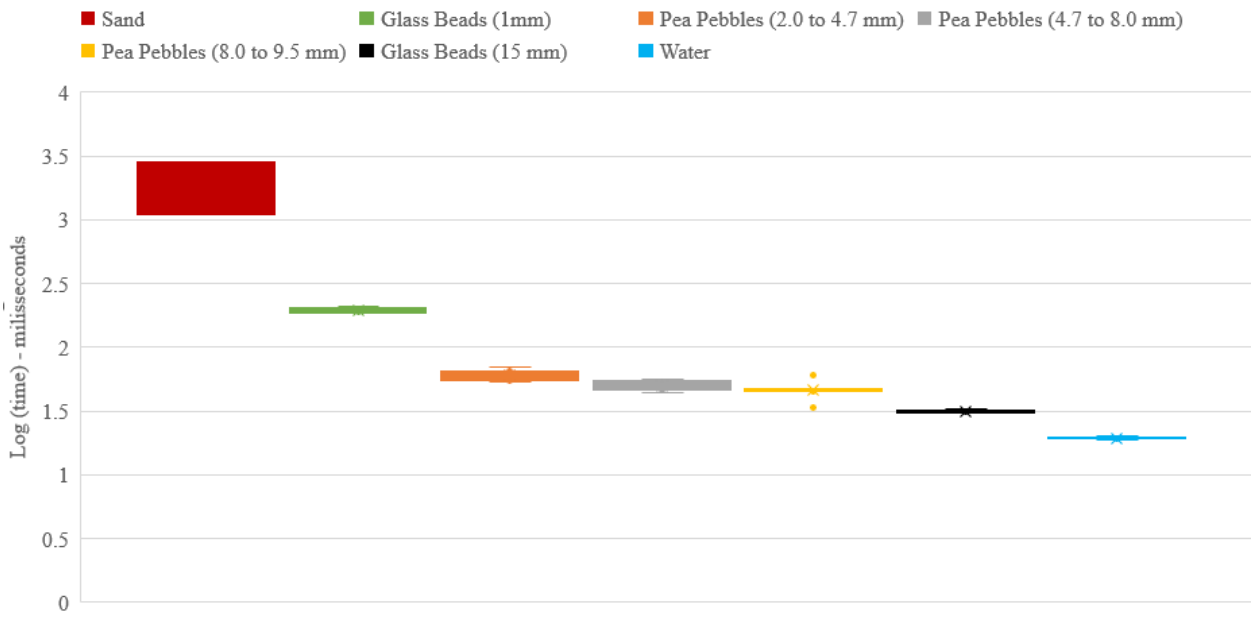

Figure 4.4: Response Time for each porous media material for the capped experiments.

The observed response time was significantly influenced by the characteristics of the porous media material, with longer pressure arrival times as the characteristic dimension of the porous media decreased. It is hypothesized that for smaller porous media, the process of pressure transmission is hindered by smaller and more numerous pores, resulting in a longer pressure transmission time. Figure 4.5 presents the relationship between the porous media hydraulic conductivity and the average pressure arrival time.

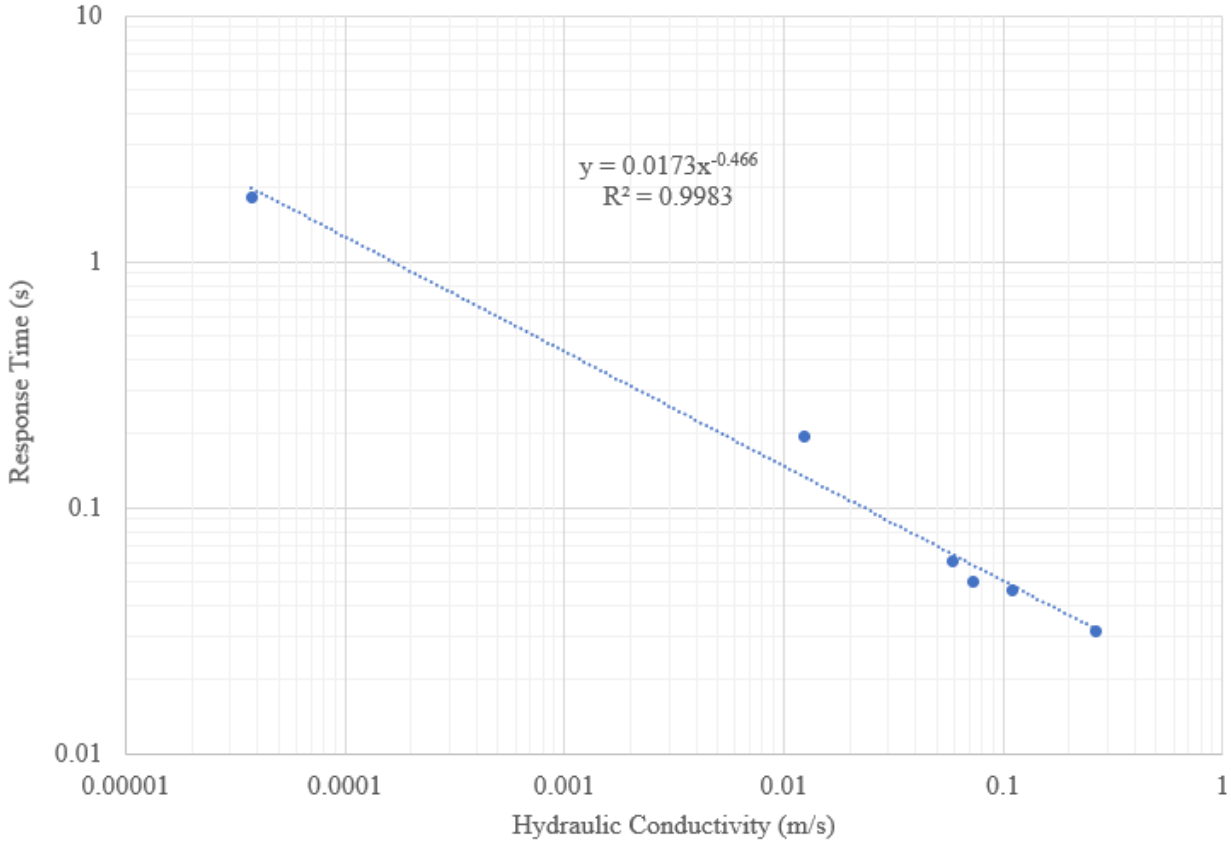

Figure 4.5: Response time vs hydraulic conductivity

Figure 4.6 presents the recorded peak pressures and the observed time for these pressures to be detected in the transducers used in the capped experiments. These results exclude the conditions where the response corresponded to traditional porous media transient flow, i.e., no pressure oscillations. It was noticed that the shortest time for peak pressures at the downstream end occurred for the pipe segments with pure water and the 15-mm glass beads. The time for the pressure peak for the pea pebble media was generally higher than the 15-mm glass beads or water, and this variable increased with a smaller pea pebble characteristic size.

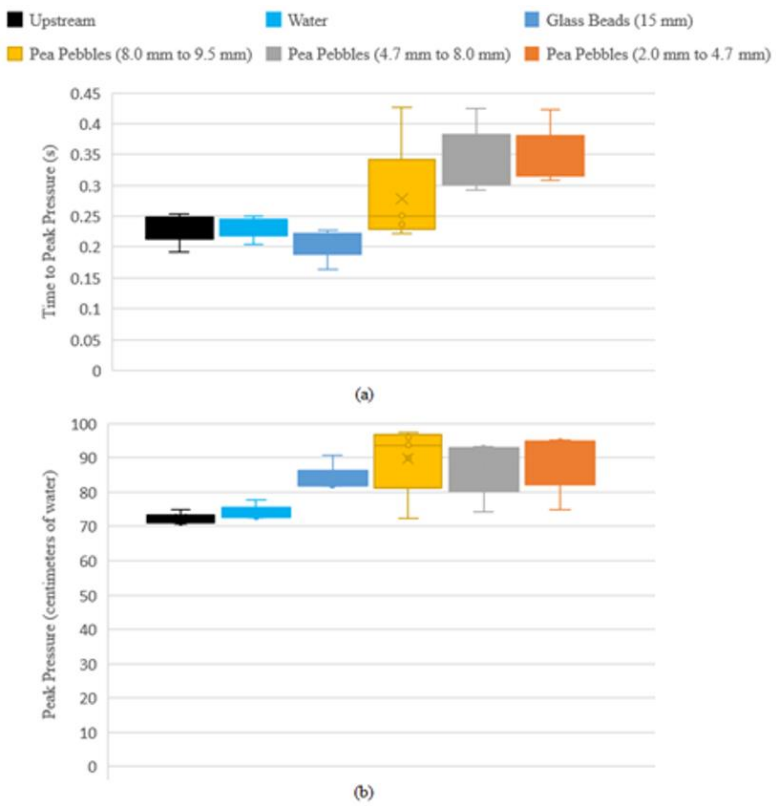

Figure 4.6: Time to peak pressure (a) and peak pressure value (b)

The peak pressure magnitude for 15-mm glass beads and pure water was very similar to the peak measured at the upstream pressure transducer, indicating a translation of the pressure pulse towards the downstream end. By contrast, these were higher for the pea pebble media, and it is hypothesized that the relatively more compacted media resulted in a less elastic overall system, which could explain higher peak pressures (Wylie et al. 1993).

While an analytical solution for the conditions with hyperbolic-nature flows is impossible, such is attainable for the two cases where typical porous media transient flows were observed. Applying the numerical methods described in the subchapter 3.7, it is possible to calculate the numerical solution of the parabolic PDE. This solution was computed for sand and glass beads of 1 mm and is presented in Figure 4.7. The coefficient $\alpha=\frac{k}{S_S}$ was calculated using the solver tool in Microsoft Excel. The minimum mean squared error method was used to select

the parameter α used in the analytical solution in order to provide the best match for the experimental measurements of pressure change.

The following sequence of figures presents a comparative analysis of numerical and experimental results: Figure 4.7a (Scenario 1) portrays a situation wherein the estimated air content stands at approximately 1%; Figure 4.7b (Scenario 2) demonstrates the scenario wherein the experimental and numerical curves exhibit the closest correspondence, signifying an air content of 10.7%. Lastly, Figure 4.7c depicts a case involving sand where the presence of air in the system is disregarded.

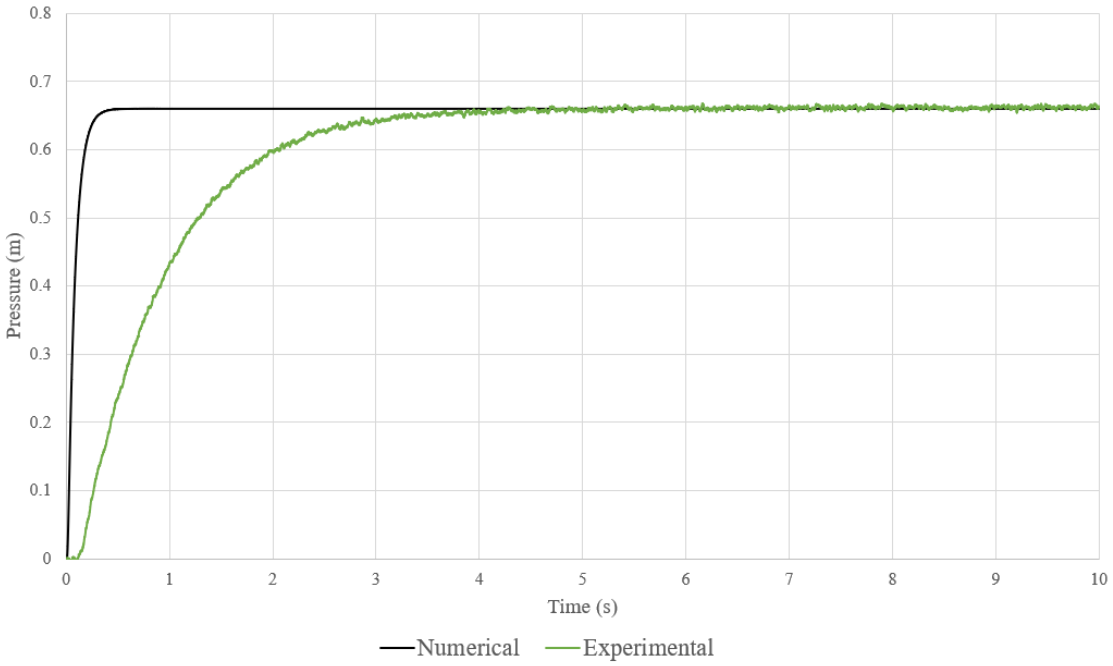

(a)

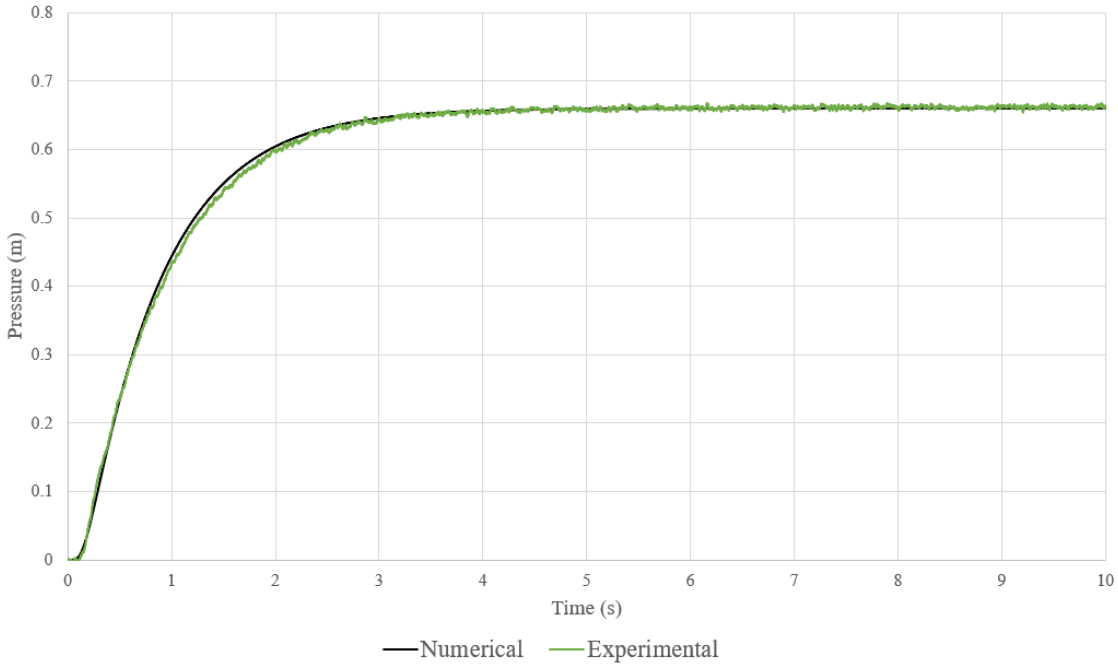

(b)

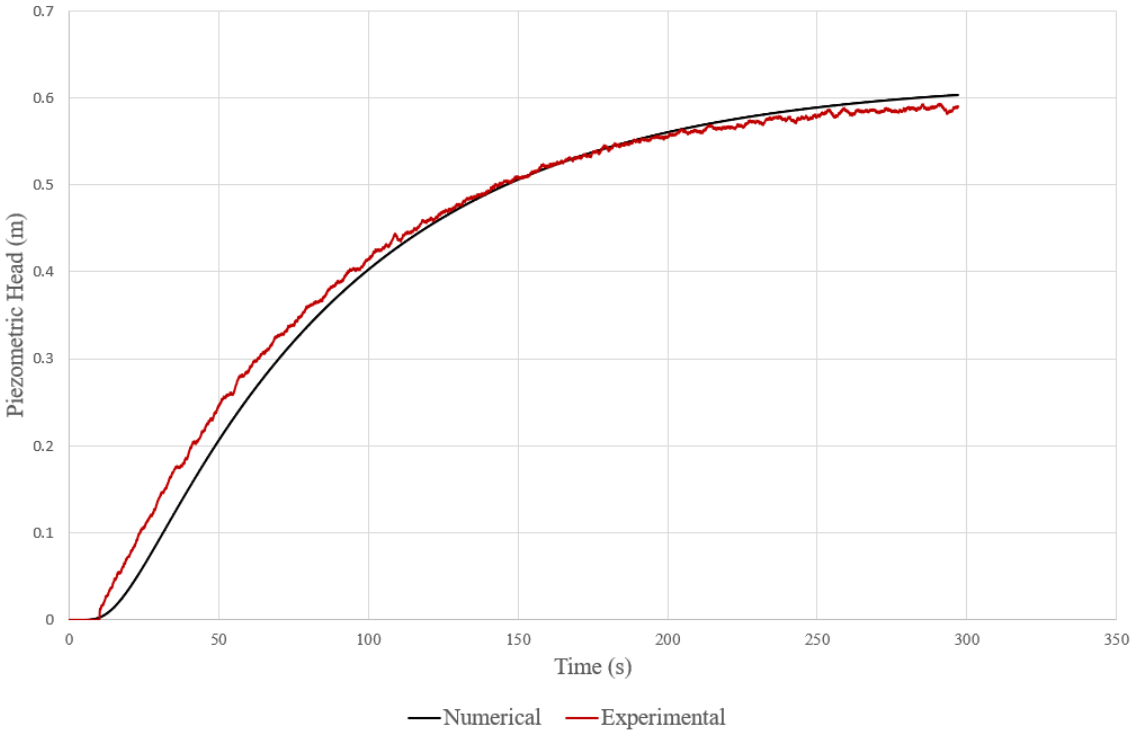

(c)

Figure 4.7: Analytical vs Experimental Results for Cap Test (a) Glass Beads 1 mm – Scenario 1 (b) Glass Beads 1 mm – Scenario 2 (c) Sand

The estimated coefficients applied to the sand material effectively yield an alpha value corresponding to a curve aligning with the experimental outcomes, displaying analogous pressure growth over time. The alpha coefficient calculated in Scenario 1 for the glass beads with a diameter of 1 mm appears to be excessively high, resulting in an analytical curve exhibiting a faster growth rate than the experimental curve. Conversely, scenario 2 shows a better alignment between the curves, but it does not assume realistic values of air content.

4.5. Surge tests: experimental results

This section presents the results from the tests where the downstream end of each pipe segment was open to the atmosphere, and the water was not allowed to escape the apparatus but instead remained on a vertical surge shaft. Furthermore, an analytical solution for the first-order ordinary differential equation that governs the surge test has been computed using Excel and incorporated into the same graph. The pressure results for all tested cases are shown in Figure 4.8, except for the sand media, since this rise was comparatively too slow to be helpful for this comparison. Also, the numerical solution for the water pipeline was not considered due to the inapplicability of Darcy's Law in such cases.

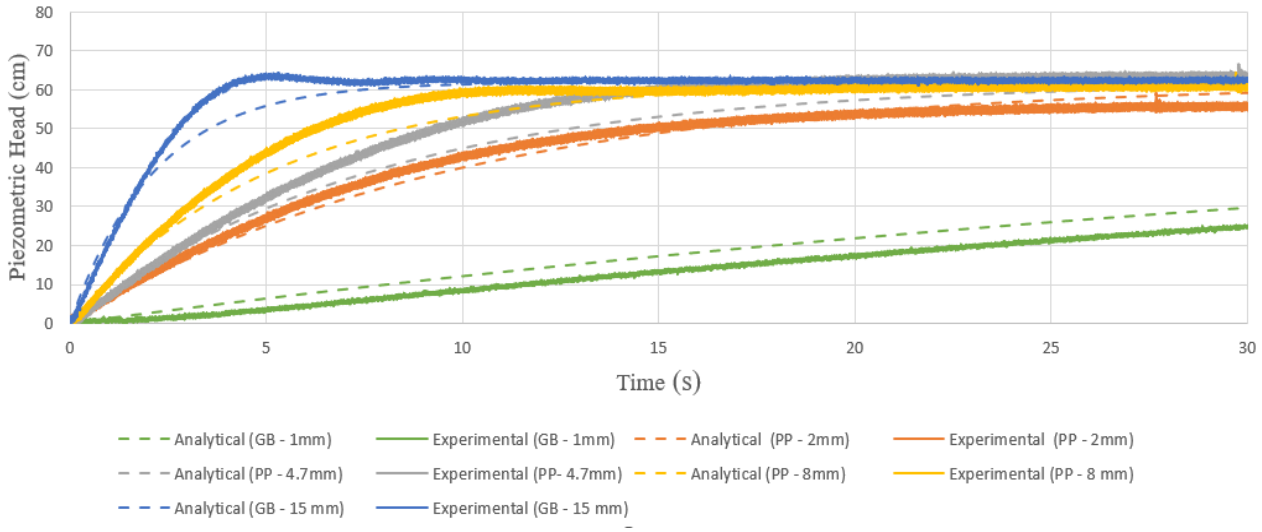

Figure 4.8:Comparison between the numerical solution and experimental pressure results for the Surge tests for all tested media.

It is possible to observe that despite the similarities in shape between both curves, a slight discrepancy exists between the experimental and analytical results. As shown in Figure 4.8, the pipelines containing glass beads of 15 mm diameter and the one without any porous media had a peak pressure exceeding the upstream reservoir pressure, similar to a surge tank inertial oscillation. This observation indicates much smaller energy dissipation in these two cases. The energy dissipation was too large for the remaining cases, preventing water from surging in the vertical towers.

4.6. Free flow tests: experimental results

The subsequent graphs present the experimental results obtained from the free flow test. The outcomes have been divided into two distinct series of experiments to enhance clarity and ease of observation. Figure *4.10* shows the results of series 1, while Figure *4.10* exhibits the results of series 2.

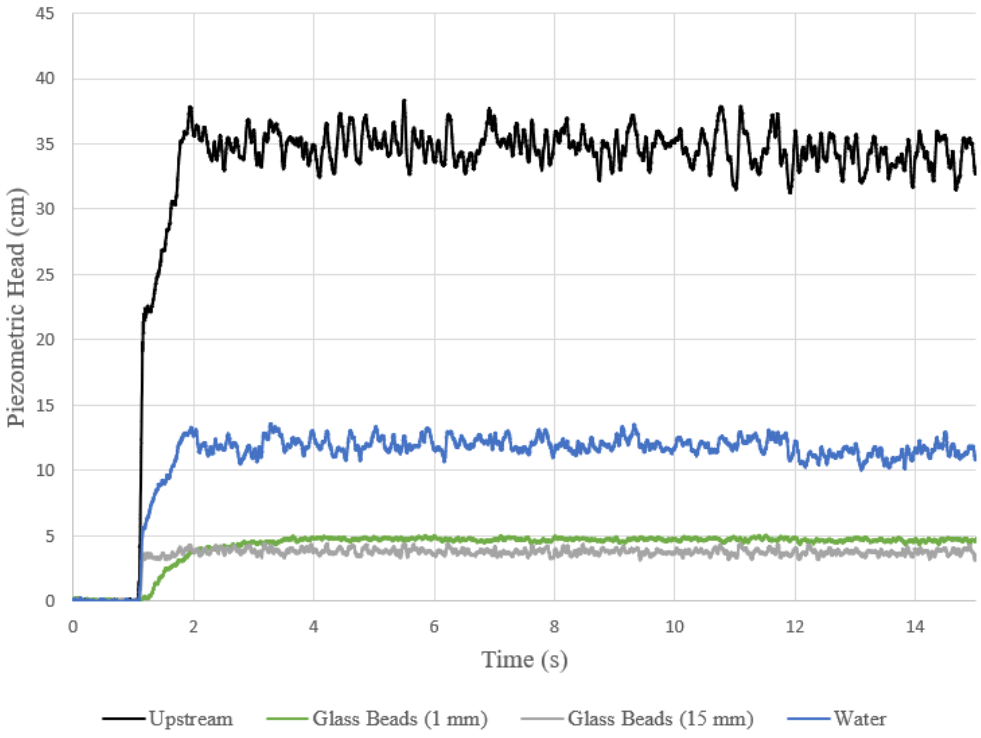

Figure 4.9: Piezometric Head over Time for Free Flow Test for series 1 of experiments.

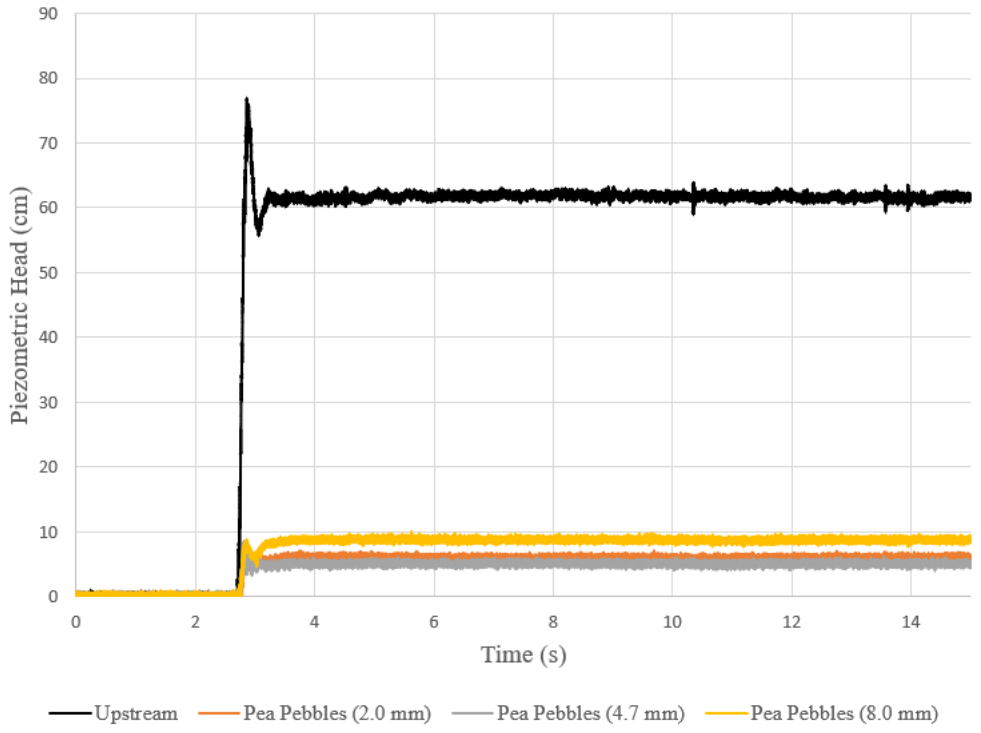

Figure 4.10: Piezometric Head over Time for Free Flow Test for series 2 of experiments.

Examining Figures 4.9 and 4.10, it becomes evident that all porous media materials exhibited diminished steady-state pressures in contrast to the case involving only water. That happens because the total head loss in the pipelines that contain porous media surpasses the total head loss observed in the absence of such media.

4.7. Study Limitations

As discussed in the Literature Review chapter, air presence can influence the experimental outcomes, notably affecting properties such as wave celerity and maximum pressure. As experiments were performed, there were challenges related to the complete removal of air within the pipelines, posing difficulties in achieving ideal test conditions. Also, the tap water employed to fill the reservoir naturally contains dissolved gases, and though it was tried to avoid this effect in the tests by introducing "aged" water in the apparatus, there was no guarantee that it was eliminated. Also, there was no anchoring for elbows and junctions, which may have impacted energy dissipation in our tests. Finally, some transducers failed during our experiments, which difficulted some data collection.

5. Conclusions

Recent studies revealed a big interest in the domain of hydraulic transients within porous media, encompassing experimental inquiries, field-based analyses, and the advancement of computational tools designed to simulate intricate physical processes occurring within such media. However, an insufficiency of investigations concurrently examining hydraulic transients in diverse porous media through the combined utilization of experimental and numerical methodologies has resulted in a discernible gap in knowledge. This lacuna pertains to the presence or absence of transitional behaviors within hydraulic transients in porous media, wherein pressure pulses deviate from conventional parabolic or hyperbolic characteristics. This absence highlights the importance of the current study, as it aims to elucidate this unexplored facet within the realm of hydraulic transients in porous media.

The present study has effectively constructed an experimental model which facilitated the determination of hydraulic conductivity across various porous media. Additionally, the model enabled the simulation of hydraulic transients under three distinct boundary conditions. Furthermore, the suite of data acquisition instruments employed herein demonstrated their utility in the comprehensive collection of pressure data during unsteady flow phenomena.

The experimental results revealed that the pressure response during the hydraulic transient exhibits a similarity between the water pipeline and porous media of diameter greater than 2 mm. This similarity persisted across all three test scenarios with distinct boundary conditions: capped outlet, open to the atmosphere with no outflow, and free flow tests.

While no instances of transitional behavior were identified within the examined porous media, it was observed that the prospect of encountering such transitional behavior may be

situated within the spectrum of porous media sizes spanning from 1 to 2 mm, or within a range of hydraulic conductivity extending from $1.24*10^{-2}$ m/s to $5.91*10^{-2}$ m/s.

The numerical solution formulated for cap and surge tests yielded a pressure curve that closely approximated the experimental results, exhibiting a reasonable level of congruence. Disparities observed within these curves could potentially be attributed to cumulative experimental inaccuracies inherent in the process of ascertaining hydraulic conductivities of the porous media. Additionally, inaccuracies in parameter estimations, encompassing porosity, air ratio, and material compressibility, might contribute to the observed discrepancies.

5.1 Future Studies

A further study is suggested to analyze the phenomenon of the transient flow under capped conditions, specifically targeting materials falling within the hydraulic conductivity interval range from $1.24*10^{-2}$ m/s to $5.91*10^{-2}$ m/s. This recommendation aims to check the potential existence of a transitional behavior wherein the transient curve deviates from the typical parabolic and hyperbolic patterns observed in the experimental outcomes.

Furthermore, it is recommended to conduct additional investigations to explore the influence of parameters, such as intruded air content and the degree of compaction of the porous media, on the experimental outcomes. Additionally, to corroborate the validity of the experimental findings and conduct hydraulic transient simulations under varied scenarios, thereby eliminating the requirement for physical experimental models, it is recommended the development of a computational approach based on the governing partial differential equations that characterize transient flow phenomena in porous media and considers the presence of air within the system. By incorporating such considerations, the computational model would be more representative

and capable of accurately capturing the complexities of hydraulic transient behavior in porous media.

6. References

Akan, A. O. (2006). “Open Channel Hydraulics.” *Butterworth-Heinemann.*

Angelakis, A. N., Voudouris, K. S., and Mariolakos, I. (2016). “Utilisation de l’eau souterraine à travers les siècles se focalisant sur les civilisations grecques.” *Hydrogeology Journal*, 24(5), 1311–1324.

ASTM. (2010). “Standard Test Methods for Measurement of Hydraulic Conductivity of Saturated Porous Materials Using a Flexible Wall Permeameter 1.” (C), 1–23.

ASTM (2017). ASTM E11-17 Standard Test Method for Sieve Analysis of Fine and Coarse Aggregates. ASTM International, West Conshohocken, PA.

Baker, S., Middleton, G., Eyles, C., Symons, S., Mcdonough, D., Rawlins, J., and Yin, C. (n.d.). “History of the Earth Volume II : Science through the Ages.” II.

Bear, J. (1979). *Hydraulics of groundwater*. McGraw-Hill.

Berre, I., Doster, F., and Keilegavlen, E. (2019). “Flow in Fractured Porous Media: A Review of Conceptual Models and Discretization Approaches.” *Transport in Porous Media*, Springer Netherlands, 130(1), 215–236.

Brandon, N.P., Brett D.J. “Engineering porous materials for fuel cell applications”. Philos Trans A Math Phys Eng Sci. 2006 Jan 15;364(1838):147-59. doi: 10.1098/rsta.2005.1684. PMID: 18272457.

Chaudhry, M. H. (1987). *Applied Hydraulic Transients*. Springer New York.

“CrunchFlow.” (2019). Earth Sciences Division Lawrence Berkeley National Laboratory, Berkeley.

Freeze, R.A. (1994), Henry Darcy and the Fountains of Dijon. Groundwater, 32: 23-

30. https://doi.org/10.1111/j.1745-6584.1994.tb00606.x

Gray, W., Miller, C. (2004). Examination of Darcy's Law for Flow in Porous Media with Variable Porosity †. Environmental Science & Technology - ENVIRON SCI TECHNOL. 38. 5895-5901. 10.1021/es049728w.

Greenkorn, R. A. (1983). *Flow Phenomena in Porous Media*. Marcell Dekker.

Grimstad, G., Amiri, S. A. G., and Nordal, S. (2019). "Relations and links between soil mechanics, porous media physics, physiochemical theory, and effective medium theory." *Frontiers in Physics*, 7(APR), 41.

Haring, R. E., and Greenkorn, R. A. (1970). "A statistical model of a porous medium with nonuniform pores." *AIChE Journal*, 16(3), 477–483.

Haynes, W. M. (2014). *CRC Handbook of Chemistry and Physics*. *CRC Handbook of Chemistry and Physics*.

Hun, B. J., Charette, M. A., and Zheng, Y. (2009). "Field, laboratory, and modeling study of reactive transport of groundwater arsenic in a coastal aquifer." *Environmental Science and Technology*, 43(14), 5333–5338.

Khalil, A., Mohammed, S., Hashaikeh, R., and Hilal, N. (2022). "Lithium recovery from brine: Recent developments and challenges." *Desalination*, Elsevier B.V., 528(February), 115611.

Li, L., Barry, D. A., Stagnitti, F., Parlange, J. Y., and Jeng, D. S. (2000). "Beach water table fluctuations due to spring-neap tides: Moving boundary effects." *Advances in Water Resources*, 23(8), 817–824.

Marcato, A., Boccardo, G., and Marchisio, D. (2022). "From Computational Fluid Dynamics to Structure Interpretation via Neural Networks: An Application to Flow and Transport in Porous Media." *Industrial and Engineering Chemistry Research*, 61(24), 8530–8541.

Martins, N. M. C., Carriço, N. J. G., Ramos, H. M., and Covas, D. I. C. (2014). “Velocity-distribution in pressurized pipe flow using CFD: Accuracy and mesh analysis.” *Computers and Fluids*, Elsevier Ltd, 105, 218–230.

Martins, N. M. C., Soares, A. K., Ramos, H. M., and Covas, D. I. C. (2016). “CFD modeling of transient flow in pressurized pipes.” *Computers and Fluids*, 126, 129–140.

Mazumder, Sandip. Numerical Methods for Partial Differential Equations: Finite Difference and Finite Volume Methods. 1st ed., Elsevier, 2015.

Mehmani, A., Prodanovic, M., Chen, J., Georgi, D., and Edwards C., (2014), "A Pore Scale Analysis of Restricted Diffusion in Shale Gas Media," SEG Global Meeting Abstracts : 559-570.

“MODFLOW 6: USGS Modular Hydrologic Model.” (2023). USGS Digital Object Identifier Catalog.

Pachaly, R. L., Vasconcelos, J. G., Allasia, D. G., and Bocchi, J. P. P. (2022). “Evaluating SWMM capabilities to simulate closed pipe transients.” *Journal of Hydraulic Research*, 60(1), 74–81.

Říha, J., Petrula, L., Hala, M., and Alhasan, Z. (2018). “Assessment of empirical formulae for determining the hydraulic conductivity of glass beads.” *Journal of Hydrology and Hydromechanics*, 66(3), 337–347.

Soares, A. K., Covas, ; Dídia I. C., and Reis, ; and Luisa Fernanda R. (2008). “Analysis of PVC Pipe-Wall Viscoelasticity during Water Hammer.”

Soares, A. K., Covas, D. I. C., and Ramos, H. M. (2013). “Damping Analysis of Hydraulic Transients in Pump-Rising Main Systems.” *Journal of Hydraulic Engineering*, 139(2), 233–243.

Song, S., Liu, Q., Cao, X., Zhang, T., and Tu, Q. (2023). “Construction of pore structure geometry model from digital images of porous media and its application in pore-scale flow simulation.” *Geoenergy Science and Engineering*, Elsevier B.V., 229(April), 212079.

Tang, Y., Q. Jiang, and C. Zhou (2016), Approximate analytical solution to the Boussinesq equation with a sloping water-land boundary, Water Resources Res., 52, 2529–2550, doi:10.1002/ 2015WR017794.

Urbanowicz, K., Stosiak, M., Towarnicki, K., and Bergant, A. (2021). “Theoretical and experimental investigations of transient flow in oil-hydraulic small-diameter pipe system.” *Engineering Failure Analysis*, 128(March).

U.S. Geological Survey. 2005. MODFLOW-2005: The U.S. Geological Survey Modular Ground-Water Model—The Ground-Water Flow Process. Techniques and Methods 6-A16. Reston, VA: U.S. Geological Survey.

Wylie, E. Benjaminm, Streeter, V. L. (1978). *Fluid Transients*.

Xiong, Q., Baychev, T. G., and Jivkov, A. P. (2016). “Review of pore network modelling of porous media: Experimental characterisations, network constructions and applications to reactive transport.” *Journal of Contaminant Hydrology*, The Authors, 192, 101–117.

Ye, Z., Fan, Q., Huang, S., and Cheng, A. (2021). “A one-dimensional line element model for transient free surface flow in porous media.” *Applied Mathematics and Computation*, 392, 125747.

Zhou, L., Cao, Y., Karney, B., Vasconcelos, J. G., Liu, D., and Wang, P. (2021). “Unsteady friction in transient vertical-pipe flow with trapped air.” *Journal of Hydraulic Research*, Taylor & Francis, 59(5), 820–834.